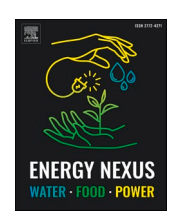
ELSEVIER

Contents lists available at ScienceDirect

Energy Nexus

journal homepage: www.elsevier.com/locate/nexus





Conceptual design and thermodynamic investigation of novel energy and fuel generation systems from municipal waste coupled with carbon capture and storage

Qurrotin Ayunina Maulida Okta Arifianti ^{a,b,*}, Stavros Michailos ^c, Maria Fernanda Rojas Michaga ^a, Karim Rabea ^{a,d}, Kevin J Hughes ^a, Lin Ma ^a, Derek Ingham ^a, Mohamed Pourkashanian ^a

- a Energy 2050, School of Mechanical, Aerospace and Civil Engineering, The University of Sheffield, Sheffield, S3 7RD, United Kingdom
- ^b Universitas Internasional Semen Indonesia, Gresik, East Java, Indonesia
- ^c School of Engineering, University of Hull, Hull HU6 7RX, United Kingdom
- ^d Department of Mechanical Power Engineering, University of Tanta, Egypt

ARTICLE INFO

Keywords:
Waste management
Waste-to-energy
Plasma gasifier
Carbon capture and storage

ABSTRACT

Waste generation and energy demand are increasing and both require innovative energy symbiosis strategies to meet climate targets. Traditional waste-to-energy processes rely on incineration, but more efficient and sustainable solutions are needed. The aim of the study is to investigate for the first time the feasibility of generating cooling, heating, power (CCHP), and liquid biomethane from plastics and food waste integrated with carbon capture and storage (CCS). The system, modelled in Aspen Plus, consists of a plasma gasifier (PG), anaerobic digester (AD), combined cycle gas turbine (CCGT), absorption refrigeration cooler (ARC), and biomethane liquefier. Two scenarios were analyzed: (1) a standalone CCHP system and (2) its integration with liquid biomethane production. Each scenario includes a baseline (without CCS), pre-combustion CCS, both with a 95% CO₂ capture fraction. Utilising 5 kg/s of plastic and 13.97 kg/s of food waste, the system generates net power (29.76–85.67 MW), cooling (2.72–4.04 MW), heating (13.99–27.87 MW), and 43.26 MW of liquid biomethane. The highest energy and exergy efficiencies achieved are 49.44% and 41.20%, with carbon emissions ranging from 0.008 to 0.247 kgCO₂/kg waste. The findings of this novel study highlight the potential of integrating several energy systems for an effective waste management strategy that can contribute to the provision of several energy vectors while the inclusion of CCS ensures that significant emission reduction can be attained.

1. Introduction

In 2015 the United Nations established seventeen sustainable development goals (SDGs) with the aim of attaining peace and prosperity for both humanity and Earth by 2030. Among these, Goal 11 seeks to ensure the sustainability of cities and human settlements by prioritising the improvement of air quality and the management of municipal and other forms of waste. Developing an efficient and environmentally friendly waste management system can be seen as a way towards achieving this goal.

Indonesia, a country with the fourth largest population in the world,

has disposed approximately 33.14 million tonnes of municipal solid waste (MSW) in 2022 [1]. Plastic and food waste accounted for 28.4% and 16.0% of the total waste composition, respectively. Food waste deposited in a landfill can release methane to the atmosphere due to natural decomposition of organic material. Further, plastic waste tends to fragment into smaller particles over time. These fragments can potentially enter water pathways, thereby endangering the habitats and ecosystems of rivers and oceans. As the population grows, the high quantity of waste may result in negative impacts, including air and water pollution, which in turn can pose dangers to human health [2,3]. Therefore, the implementation of effective waste management practices becomes crucial to mitigate the quantity of waste generated and protect

E-mail address: qamarifianti1@sheffield.ac.uk (Q.A.M.O. Arifianti).

^{*} Corresponding author at: Energy 2050, Department of Mechanical Engineering, Faculty of Engineering, University of Sheffield, Sheffield S3 7RD, United Kingdom.

Nomenclature		Acronym	Acronyms		
		AD	anaerobic digester		
Ė	energy flow rate	AFR	air fuel ratio		
Ėx	exergy flow rate	ARC	absorption refrigeration cooler		
$\dot{E}x_0$	standard molar chemical exergy	CC	combustion chamber		
$\dot{E}x_D$	exergy destruction	CCGT	combined-cycle gas turbine		
m m	mass flow rate	CCHP	combined cooling heating power		
	heat flow rate	CCS	carbon capture storage		
Q		ER	equivalence ratio		
R	universal gas constant	GT	gas turbine		
T	temperature	HRSG	heat recovery steam generator		
Ŵ	work rate	HPWS	high Pressure water scrubber		
η_{en}	energy efficiency	LHV	lower heating value		
η_{ex}	exergy efficiency	LSL	lean solvent loading		
Subscrip	ts	PG	plasma gasifier		
comp	compressor	RSL	rich solvent loading		
en	energetic	SAMR	steam to air mass ratio		
eva	evaporator	SOFC	solid oxide fuel cells		
ex	exergetic	SRD	specific reboiler duty		
fw	food waste	ST	steam turbine		
gen	generator	SFR	steam to feedstock ratio		
hpt	high pressure turbine	HTR	hot temperature reactor		
hpp	high pressure pump	HTZ	hot temperature zone		
ipt	intermediate pressure turbine	LCA	life cycle assessment		
ipp	intermediate pressure rurbine	Li-Br	lithium bromide		
liq	liquid	LTR	low temperature reactor		
lpt	low pressure turbine	LTZ	low temperature zone		
lpp	low pressure pump	MCFC	molten-carbonate fuel cell		
ml	methane liquifier	ML	methane liquefier		
postcc	post carbon capture	MSW	municipal solid waste		
precc	pre carbon capture	MW	megawatt		
pw	plastic waste	PSA	pressure swing adsorption		
ref	refrigeration	WGS	water gas shift		
SC	scenario	WGSR	water gas shift reaction		
30	SCHAITO	wt	weight		
		XFHE	cross flow heat exchanger		

the environment against pollution caused by waste.

Waste can be utilized as a valuable energy source due to its relatively high energy content. Plastic waste is characterized by a higher heating value (HHV) ranging from 23.97 to 46.48 MJ/kg [4,5]. Meanwhile, the lower heating value (LHV) of food waste ranges from 10.54 to 25.32 MJ/kg [6], based on its composition. In the waste management system, the waste can be converted into electrical and thermal energy using either thermochemical or biochemical process. Plasma gasification is a thermochemical process that employs plasma as the primary heating source, typically produced by direct current (DC) non-transferred arc plasma torches at ~4000°C [7]. It offers several notable advantages in waste treatment processes [8]. One such advantage is their ability to generate syngas with a substantial energy content, primarily consisting of H₂ and CO even when utilising low grade fuels [9]. The syngas produced through plasma gasification is cleaner than that generated through conventional gasification [10]. Simultaneously, the inorganic compounds are melted and transformed into a dense, chemically stable, and non-leaching vitrified slag, which possesses potential applications, particularly in the field of construction materials [11].

The application of a plasma gasifier (PG) to convert plastic waste into syngas can be considered as a more effective option since the extreme operating temperature can lead to a complete decomposition of plastic waste into its basic molecular composition. Some previous studies observed the utilization of plastic waste in the PG. For example, Cudjoe and Wang [12] compared the energy, economic and environmental evaluation of plasma gasification and incineration of plastic waste,

concluding that plasma gasification outperforms incineration of plastic waste in each evaluation. Mazzoni and Janajreh [13] studied the gasification of mixed plastic waste and municipal solid waste at different ratios in an integrated plasma gasification combined cycle (IPGCC). They found that a mixture of 30% plastic waste and 70% MSW yielded the best plant performance, with an efficiency of 38% when pure oxygen was used as the plasma gas. Kwon and Im [14] compared the thermodynamic performance of IPGCC with a thermal plasma and non-thermal plasma, fed with plastic waste. Their study revealed that IPGCC with thermal plasma and non-thermal plasma, achieving cold gas efficiencies (CGE) of 60–80%, exhibited higher energy efficiency than traditional integrated gasification combined cycle (IGCC) systems.

The present study addresses not only the utilization of plastic waste but also explores the potential of food waste into energy. The focus on food waste and plastic waste specifically addresses two of the most problematic waste streams in terms of volume and environmental impact. This targeted approach ensures the research is highly relevant to current waste management challenges. However, due to its high moisture content (approximately 70% to 90%), food waste is unsuitable for gasification [15]. For an effective gasification, the feedstock moisture content must be 30% or lower [16]. An anaerobic digester (AD) offers a more suitable method for converting high-moisture content of food waste into biogas with the help of microorganisms [17,18]. Integrating the PG (for plastic waste) and AD (for food waste) could lead to improved resource utilization. However, up to now, to the best of the author knowledges, no studies have been conducted on the coupling of

the PG and AD.

There is a growing research interest in combining various processes to convert a single source of fuel energy into multiple useful energy outputs, such as cooling, heating, electricity, fuel and fresh water [19-21]. These integrated energy systems are built to improve energy efficiency, reduce fuel consumption and cut down the amount of greenhouse gas emissions [22,23]. A combined cooling, heating, power (CCHP) system, which is referred to as trigeneration, can simultaneously provide cooling, heating, and electricity. Although the CCHP system can bring several notable advantages, from the literature review, it was revealed that only two publications reported the application of the PG in a CCHP system. The first study by Zhang et al. [24] proposed a CCHP system consisting of a PG fuelled by municipal sludge, solid oxide fuel cell (SOFC), gas turbine (GT), supercritical carbon dioxide (S-CO₂) cycle, and double-effect absorption refrigeration cooler (ARC). The second study by Zhang et al. [25] reported the performance of the CCHP system including a PG fed with food waste, SOFC, GT, S-CO2 cycle, cascade absorption refrigeration/dehumidification. It is worth mentioning that the food waste used in [25] was dried to a final moisture content of less than 2%. From the reviewed literature and other existing studies, it is evident that research on PG systems has primarily focused on the production of syngas [26–29], hydrogen [30–33], electricity [11,34–40], combined hydrogen and electricity [9,41,42], CCHP [24,25] and methanol [43,44], with limited exploration of their integration into

The integration of carbon capture and storage (CCS) technology is essential for reducing carbon emissions in energy systems and aligns with the climate targets set by the International Energy Agency (IEA) [45] and the Intergovernmental Panel on Climate Change (IPCC) [46]. To achieve low-carbon energy production, CCS must be incorporated into plasma gasification and anaerobic digestion processes, along with their downstream energy applications. While previous studies have explored CCS implementation in plasma gasification-based systems for various waste feedstocks [9,24,33,47-49], only two studies have specifically focused on plastic waste as a primary feedstock [9,49]. The first study utilized a monoethanolamine (MEA)-based post-combustion CCS system with a 90% carbon capture fraction, restricting its energy output to hydrogen and electricity [9]. The second study employed an MEA-based pre-combustion CCS system with the same 90% capture fraction, also producing only hydrogen and electricity [49]. In contrast, the current study extends this research by evaluating both pre-combustion and post-combustion CCS configurations with an improved 95% carbon capture fraction. By comparing these configurations, this study aims to identify the most efficient integration strategy for maximizing carbon mitigation in waste-to-energy systems.

In this study, a CCHP system with liquid fuel generation is proposed, integrating CCS to enhance sustainability. The system utilizes syngas from plasma gasification of plastic waste and biogas from anaerobic digestion of food waste, selected for their dominance in landfill waste composition. This dual-feedstock integration improves resource efficiency and energy recovery in waste-to-energy applications.

The system is scalable and adaptable, and it has the potential to support centralised grid integration in urban areas as well to serve as a decentralized energy source for off-grid regions. The system can be implemented in hot-humid climates as waste heat from gas turbine exhaust drives an absorption refrigeration cooler (ARC) and this can reduce electrical cooling demand. At the same time, in colder regions, it can be used for district heating to provide low-carbon thermal energy. Additionally, liquid biomethane production offers a sustainable alternative to liquefied petroleum gas (LPG). Thus, it can reduce dependence on fossil fuels and facilitate energy security. Beyond energy recovery, the system supports circular economy principles by repurposing slag for construction materials and digestate as agricultural biofertilizers. The proposed conceptual designs have the potential to set the basis for subsequent detailed engineering studies and inform policy making about sustainable waste management routes that can offer deep

decarbonisation.

While this study is applied in the context of Indonesia, the system configuration is adaptable and can be applied in other regions facing similar waste and energy challenge. Recent studies have examined municipal solid waste management across various national and urban contexts. For example, Albizzati et al. [50] conducted a multi-country evaluation of waste treatment strategy in the EU using life cycle assessment (LCA), and life cycle costing, primarily focusing on conventional methods like composting, recycling, and incineration. However, their model does not consider mixed feedstocks or advanced energy recovery configurations and emission mitigation technologies, such as multi- output energy systems integrated with CCS, as implemented in the current study. Meanwhile, Rafiquee and Shabbiruddin [51] observed the most suitable smart waste management system in Patna, India by using multi-dimensional criteria that included economic, technical, environmental, and public acceptance considerations. However, their study was limited to evaluating waste handling and collection infrastructure, without examining waste conversion technologies or energy recovery processes.

Kua et al. [52] used life cycle assessment to evaluate greenhouse gas mitigation potential in Singapore by treating plastic, food, and sewage sludge using anaerobic digestion and pyrolysis. While their study addressed the climate benefits of managing multiple waste types, it did not include any form of carbon capture and was limited to heat and electricity generation, without multi-vector energy outputs, such as cooling or liquid fuels. In contrast, the current study combines plastic and food waste in a dual-feedstock configuration, using plasma gasification and anaerobic digestion, respectively. The system produces electricity, heating, cooling, and liquid biomethane, while also incorporating both pre-combustion and post-combustion CCS at 95% efficiency.

A comprehensive thermodynamic assessment is conducted to evaluate component- and system-wide performance, which focuses on energy and exergy efficiency, heat integration, and process optimisation to enhance overall system effectiveness. The novelty of this study lies in its dual-feedstock and multi-output approach, which can identify the optimal configurations for maximum efficiency and emissions reduction. This work provides a technically rigorous foundation for future economic and environmental assessments of sustainable waste to energy systems.

2. Methodology

2.1. System description

An integrated system for generating electricity, cooling, heating, and liquid fuel has been designed for one of Indonesia's largest landfills. The Benowo landfill, located in Surabaya—the country's second most populous city with approximately 2.8 million residents as of the 2020 census—covers an area of about 37.4 hectares [53,54]. In 2020, the landfill received 2,222.62 tonnes of waste daily, predominantly composed of 54.31% food waste and 19.44% plastic waste, with the remainder consisting of paper, twigs, rubber, glass, and fibres [1]. Currently, the waste-to-energy system at Benowo is limited to electricity generation, leaving significant potential for expansion into other energy outputs [1].

The energy needs of the surrounding community extend beyond electricity to include cooling, heating, and fuel. In a country with a hothumid climate like Indonesia, the demand for cooling energy is expected to rise significantly [55,56]. Waste heat recovered from the landfill's power plant offers a sustainable solution to address these demands, such as providing energy for space cooling. Additionally, the landfill's proximity to coastal areas presents an opportunity to support the region's salted fish industry, one of Indonesia's key export products. The traditional sun-drying process for fish poses hygiene risks, but utilizing recovered waste heat for fish drying can improve product quality and

safety.

Moreover, LPG, a widely used fuel in Indonesian households, can be substituted with liquid biomethane derived from food waste, reducing dependence on natural gas and offering a sustainable alternative. Beyond energy recovery, the system's byproducts present additional value. Slag produced by the PG can be used as a construction material, while dried digestate from anaerobic digestion can serve as an organic fertilizer, supporting circular economy principles.

In response to the growing need for sustainable energy solutions derived from waste, this research proposes two scenarios for optimizing energy recovery and reducing environmental impacts through advanced waste-to-energy technologies. The first scenario involves the application of a CCHP system. Meanwhile, the second scenario integrates the CCHP system with liquid biomethane production. Both scenarios assume the production of syngas and biogas, as shown in Figs. 1 and 2. Specifically, syngas is generated by feeding shredded plastic waste to the PG, and biogas is produced from the anaerobic digestion of food waste. To evaluate the impact of carbon emissions, each scenario examines three configurations: a baseline without CCS, one with pre-combustion CCS

(pre-CCS), and one with post-combustion CCS (post-CCS). The $\rm CO_2$ emissions captured from the system are transported to the nearest $\rm CO_2$ storage site, the Bawean Basin, which has a storage capacity of 1.16 gigatonnes and is located approximately 150 kilometres from the landfill [57].

2.1.1. Scenario 1 (CCHP)

Fig. 1a–1c are the visual representation of the three configurations of the first scenario. The first configuration as shown in Fig. 1a is the simplest one and serves as the basis for further comparisons. In this set up, a mixture of raw biogas and syngas drives a combined-cycle gas turbine (CCGT) which utilizes a gas turbine (top cycle) and a steam turbine (bottom cycle) to generate electricity. The residual heat in the flue gas exiting the CCGT unit can be recovered in a single-effect ARC to produce cooling suitable for a housing area. Additionally, the waste heat generated from the ARC can be used in industrial applications such as fish drying.

The second configuration, illustrated in Fig. 1b, introduces two additional subsystems, highlighted within the red dotted box. These

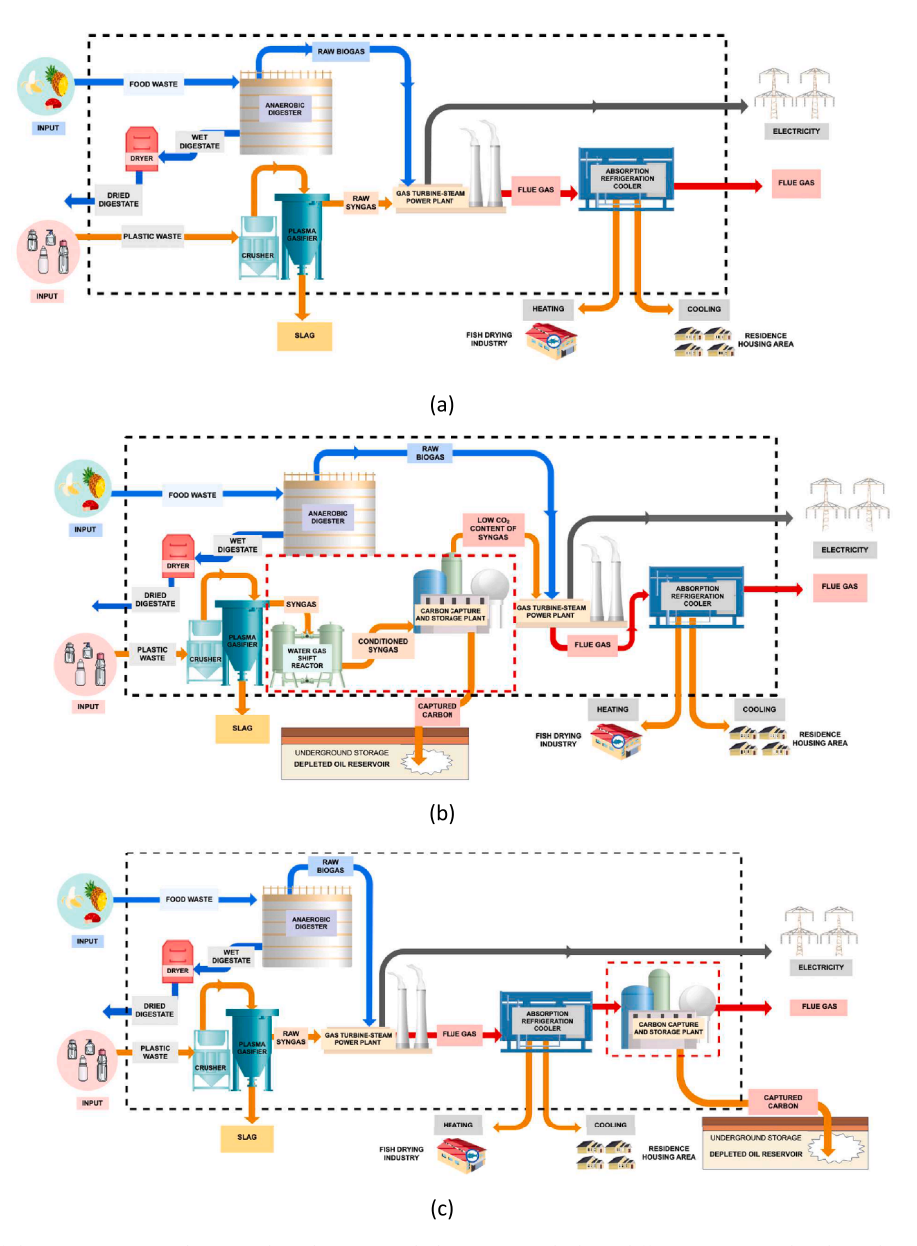


Fig. 1. Process schematic of the Scenario 1 (products: cooling, heating, and electricity) with three different cases: (a) baseline, (b) integrated with pre-CCS, (c) integrated with post CCS.

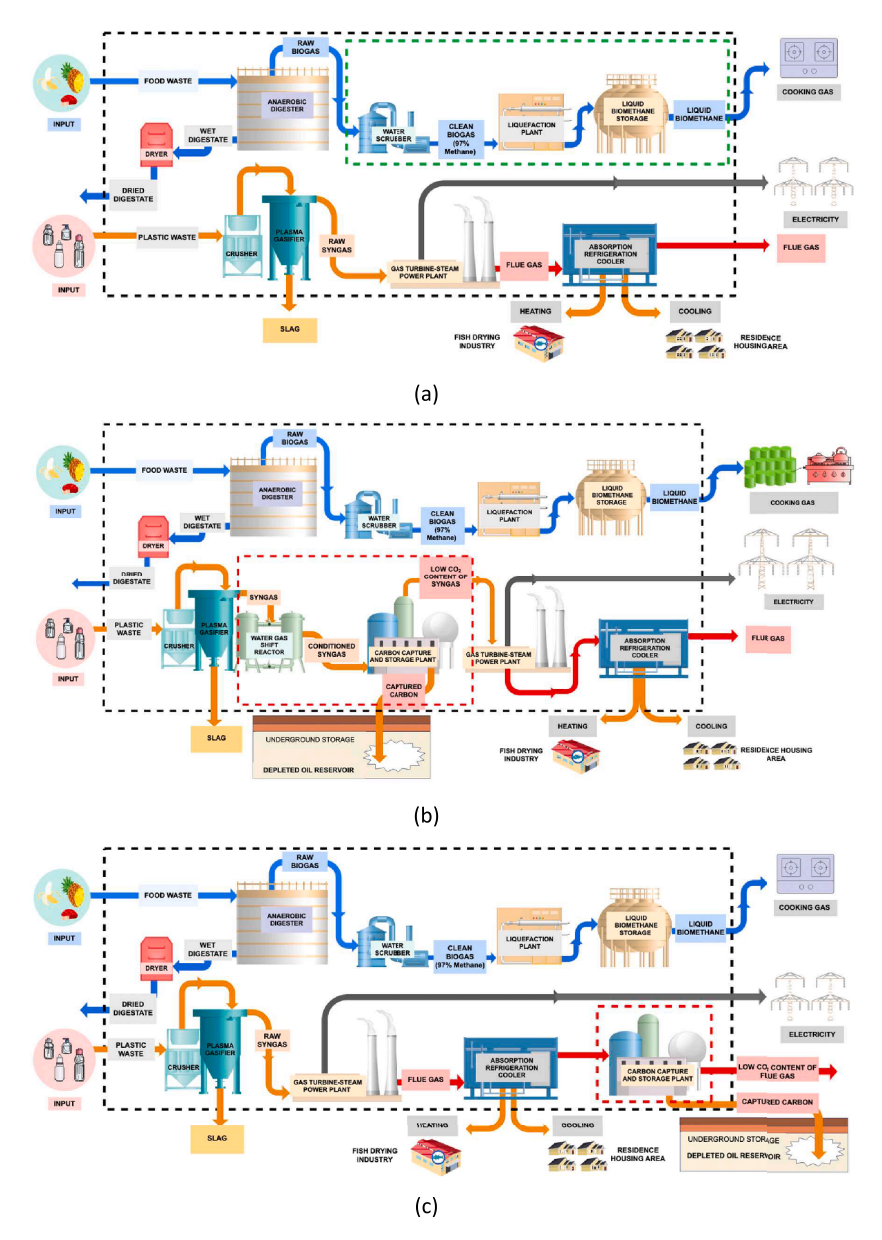


Fig. 2. Process schematic of the Scenario 2 (products: cooling, heating, electricity, and liquid fuel) with three different cases: (a) baseline, (b) integrated with pre-CCS, (c) integrated with post CCS.

include a water gas shift (WGS) reactor and a pre-CCS plant. In this setup, the raw syngas is sent to the WGS reactor before it is mixed with the raw biogas. Through the WGS reactor, the CO present in the syngas is transformed into $\rm CO_2$, hence raising the concentration of $\rm CO_2$ in the gas stream. The resulting syngas is then mixed with the raw biogas and fed to the pre-CCS plant before combustion in the CCGT.

The final configuration, shown in Fig. 1c, differs from the others by incorporating a post-combustion carbon capture (post-CCS) plant. Instead of releasing the flue gas directly into the atmosphere, as in the first configuration, the flue gas passes through the post-CCS plant, which is located after the ARC. The post-CCS system captures CO₂ from the flue gas before it is released, as indicated by the red dotted box in Fig. 1c.

2.1.2. Scenario 2 (CCHP and fuel production)

The three configurations in the second scenario are depicted in Fig. 2a–2c. In this scenario, instead of using the raw biogas produced in the AD unit as a fuel for the CCGT, it is purified in a high-pressure water scrubber (HPWS) to increase the methane concentration. The resulting biomethane is then directed to a methane liquefier (ML) to liquify

biomethane, which can be used as cooking gas. In Scenario 2, the CCHP system is fuelled solely by syngas to generate electricity. Similar to the Scenario 1, before the flue gas is released from the CCHP, its heat is used by the ARC to generate cooling, and the heat rejected by the ARC is utilized for fish drying.

Fig. 2a illustrates the baseline configuration, where the flue gas is released directly into the atmosphere. The primary distinction from Scenario 1 is marked by the green dotted box in Fig. 2a, which highlights the additional process of converting biogas into liquid biomethane. Fig. 2b shows the configuration integrated with a pre-CCS plant, including the WGS reactor and pre-CCS system, as indicated by the red dotted box. In this configuration, the pre-CCS system only removes carbon from the syngas before it enters the CCHP.

Finally, Fig. 2c depicts the configuration with the post-CCS plant added to the baseline system, as shown by the red dotted box. The post-CCS system captures carbon from the flue gas produced by syngas combustion before it is released into the atmosphere.

2.2. System modelling

The investigated processes were modelled in Aspen Plus V12.1. In order to adapt to standard operational parameters, it was essential to refer to relevant technical literature. Table 1 displays the important process design parameters utilised in the modelling. The detailed Aspen model is further explained in the **Supplementary Information Section S.1**.

2.3. Thermodynamic evaluation

Table 2 presents the proximate and ultimate analysis of the food waste and mixed plastic waste used in the current study. The chemical composition of food waste and mixed plastic waste is inputted into the anaerobic digestion and plasma gasification models, respectively.

In order to assess the thermodynamic efficiency of each system, it is

 Table 1

 Process design parameters used in the Aspen Plus modelling.

Process	Conditions
Pretreatment	Crusher [58]: Model = gyratory crusher, resulting in the particle
	size reduction to 1 mm.
	Electricity required for grinding [58]:
	$\dot{W}_{1} = 50 \frac{\text{kWh}}{\text{m}}$
	$\dot{W}_{elc,consumption} = 50 \frac{\text{KWh}}{\text{ton of feedstock}}$
PG	Model [59]: Air plasma gasifier combined with the steam
	injection.
	Plasma torch temperature [60]: 4000°C.
	ER and SAMR ratio of plasma gasifier = 0.14 and 0.396,
	respectively. (ER and SAMR ratio were chosen iteratively until the temperature of HTZ reaching 2500°C).
	SFR = 0.8 .
	Steam temperature [59] = 4000° C.
	HTZ temperature $[60] = 2500^{\circ}$ C.
	LTZ temperature [60]= 1250°C.
AD	Digestion temperature = 38° C
	The dilution ratio [61]: Food waste:water = 2.64:1, kg/kg.
	Heating demand during the digestion process [62]:
	$\dot{Q}_{digestion} = 10\%.\dot{E}_{biogas}$
HPWS	Compressor 1 [63]: $P_{output} = 5$ bar
	Compressor 2 [63]: $P_{output} = 10$ bar
	Absorber [63]: $P = 10$ bar; $T = 20^{\circ}$ C
	Stripper [63]: $P = 1$ bar; $T = 20^{\circ}$ C
	Flash [63]: $P = 3$ bar; $T = 20^{\circ}$ C
GT power	Air compressor [64,65]: pressure ratio = 19.5; $\eta_{isentropic} = 85\%$;
cycle	$\eta_{mechanical} = 98.65\%$; $\dot{m}_{air\ comp}$ is determined until temperature of
	flue gas prior to gas turbine reach =1350°C.
	Combustion chamber [64]: fuel pressure = 26.83 bar.
	Gas turbine [64]: $P_{output} = 1.065 \text{ bar}; \eta_{isentropic} = 89.769\%;$
	$\eta_{mechanical} = 98.65\%$.
ST power	Steam turbine [66]:
cycle	HP: $P_{input} = 180.2$ bar; $P_{output} = 28.8$ bar; $\eta_{isentropic} = 88.03\%$.
	IP: $P_{input} = 28.8 \text{ bar}$; $P_{output} = 3.907 \text{ bar}$; $\eta_{isentropic} = 92.37\%$.
	LP: $P_{input} = 3.907 \text{ bar}$; $P_{output} = 0.0483 \text{ bar}$; $\eta_{isentropic} = 93.67\%$.
ARC	Working fluid [67]: LiBr/H ₂ O; $m_{LiBr-H_2O}/m_{fluegas} = 0.1$; LiBr
	concentration in a basic solution $= 57.4\%$.
	Pump [67,68]: $P_{input} = 0.00672$ bar; $P_{output} = 0.07461$ bar;
	$\eta_{isentropic} = 75\%; \eta_{driver} = 95\%.$
	Valve [67,68]: $P_{input} = 0.07461$ bar; $P_{output} = 0.00672$ bar.
	Designated temperature
	$T_{air,cooling} = 21^{\circ}$ C (cooling for residence house)
	$T_{air,heating} = 52^{\circ}$ C (heating for fish drying)
ML	Methane compressor [69]: $P_{output} = 200 \text{ bar}$
CCS unit	Pre-CCS
	Absorber: $H = 25 \text{ m}$; $D = 5 \text{ m}$
	Stripper: $H = 15 m$; $D = 3.5 m$; $P = 2.4 bar$ Post-CCS
	Absorber: $H = 25 m$; $D = 8.5 m$
	Stripper: $H = 25 \text{ m}$; $D = 3.5 \text{ m}$; $P = 2.6 \text{ bar}$
	Carbon sequestration
	Compressor [70]: multistage; $P_{outlet, 1} = 7$ bar; $P_{outlet, 2} = 24$ bar;
	$P_{outlet, 3} = 83 \text{ bar}$
	Pump [70]: <i>P</i> _{outlet} = 153 bar

 Table 2

 Proximate and ultimate analysis of the feedstock used in the study.

Characteristics	Food Waste [71]	Mixed Plastic [5]
Proximate Analysis (wt.%, as received)		
Moisture	76.47	0.6
Ash	14.81	13.3
Volatiles	83.1	85.7
Fixed Carbon	2.09	0.4
Ultimate Analysis (wt.%, as dry basis)		
Carbon	40.03	79.77
Hydrogen	5.72	15.47
Nitrogen	1.9	2.76
Oxygen	37.08	2
Sulfur	0.46	0
Chlorine	0	-

necessary to determine the energy and exergy content of all process streams. The energy content of the feedstock can be determined by employing the subsequent calculation:

$$\dot{E}_{feedstock} = \dot{m}_{feedstock}.LHV_{feedstock} \tag{1}$$

where $\dot{m}_{feedstock}$ is the mass flow rate of feedstock (kg); LHV_{feedstock} is the lower heating value of feedstock which can be obtained from the equation as follows:

$$\begin{split} LHV_{feedstock} = 0.339 \ \times \ \%C + 1.029 \ \times \ \%H + 0.109 \ \times \ \%S - 0.112 \\ \times \ \%O - 0.025 \ \times \ \%W \ [MJ \, / \, kg] \end{split} \label{eq:condition}$$
 (2)

where C, H, S, O, and W are the mass fraction of carbon, hydrogen, sulfur, oxygen, and water in the dry feedstock as received (%), respectively. The properties of each feedstock can be seen from Table 2.

For the exergy content of the feedstock, the empirical correlation proposed by Szargut [72] is employed to determine the specific chemical exergy of solid fuels, which is afterwards utilized for the computation of the chemical exergy of the solid waste. The exergy rate of the feedstocks can be mathematically represented as follows:

$$\dot{e}x_{feedstock} = \lambda \ LHV_{feedstock} \tag{3}$$

$$\dot{E}x_{feedstock} = \dot{m}_{feedstock} \ \dot{e}x_{feedstock}$$
 (4)

where $\dot{e}x_{feedstock}$ is the specific chemical exergy of the feedstock (MJ/kg); $\dot{E}x_{feedstock}$ is the exergy content of the feedstock (MW). Here, λ is the statistical correlation that can be calculated based on the ratio of $\frac{O}{C}$:

$$\lambda = 1.0438 + 0.0158 \frac{H}{C} + 0.0813 \frac{O}{C} \text{ for } \frac{O}{C} \le 0.5$$
 (5)

$$\lambda = \frac{1.0414 + 0.0177 \left(\frac{H}{C}\right) - 0.3328 \left(\frac{O}{C}\right) \left[1 + 0.0537 \left(\frac{H}{C}\right)\right]}{1 - 0.4021 \left(\frac{O}{C}\right)} \text{ for } 0.5 \le \frac{O}{C}$$

$$< 2$$

. . .

(6)

where H, O, C, are the percentage of hydrogen, oxygen, and carbon in the ultimate analysis, respectively.

For the output gas generated through gasification and anaerobic digestion, the energy content of individual gases can be determined by employing the following equation:

$$\dot{E}_{gas} = \dot{m}_{gas}.LHV_{gas} \tag{7}$$

$$LHV_{gas} = 1.20087 \; (\%H_2) + 0.10160(\%CO) + 0.49853(\%CH_4) \; [\text{MJ}/\text{kg}]$$
(8)

where \dot{E}_{gas} is the energy content of the generated gas from either the AD or PG (MW); \dot{m}_{gas} is the mass flow rate of the gas; H_2 , CO, and CH_4 are the mass fraction of hydrogen, carbon monoxide, and methane in the product gas (%), respectively; LHV_{gas} is the lower heating value of gas (MJ/kg).

The following equations could be used to calculate the exergy content of the generated gas.

$$\dot{e}x_{gas} = \sum_{i}^{n} y_{i}ex_{0,i} + RT_{0} \sum_{i}^{n} y_{i}lny_{i}$$
 (9)

$$\dot{E}x_{gas} = \dot{m}_{gas}\dot{e}x_{gas} \tag{10}$$

Where $\dot{e}x_{gas}$ is the exergy content of the generated gas (kJ/kg); y is the molar fraction of each substance; and ex_0 is the standard molar chemical exergy (kJ/kmol) at 298 K and 1 atm in which the value of each gas composition can be seen in Table 3.

After the quantification of the energy and exergy flows, it is possible to calculate relevant efficiencies.

• Plasma gasification

The equivalence ratio, a critical parameter in gasifier design, is defined as the ratio of the actual air-fuel ratio to the stoichiometric air-fuel ratio [74].

$$ER(<1.0)_{gasification} = \frac{(\dot{m}_{air})_{actual}}{(\dot{m}_{air})_{stoichiometric}}$$
(11)

where $\dot{m}_{air}/\dot{m}_{PW}$ is the actual ratio of mass flow rate air to plastic waste and $(\dot{m}_{air}/\dot{m}_{PW})_{stoic}$ is the stoichiometric ratio of mass flow rate air to plastic waste. The steam to air mass ratio (SAMR) is a dimensionless parameter that is frequently employed to quantify the rate at which steam is supplied in the air and steam gasification process [59].

$$SAMR = \frac{\dot{m}_{steam}}{\dot{m}_{oir}} \tag{12}$$

In the plasma gasification, the energy conversion efficiency $(\eta_{en,pg})$ is calculated as the ratio of the energy content of the syngas to the energy content of solid waste and the electricity consumed for plasma torch during the process and it can be written as follows [60]:

$$\eta_{en.pg} = \frac{\dot{E}_{syngas}}{\dot{E}_{pw} + \dot{Q}_{preheat,air} + \dot{Q}_{preheat,water} + \frac{P_{torch}}{\eta_{torch}}}$$
(13)

where \dot{E}_{pw} and \dot{E}_{syngas} are the energy content of plastic waste and syngas which can be calculated using Eqs. (1) and (7), respectively, P_{torch} is the torch power (MW), η_{torch} represents the thermal efficiency of torch, which is set to 90%, $\dot{Q}_{preheat,air}$ and $\dot{Q}_{preheat,water}$ represent the heat utilized to preheat the air (prior to entering the torch) and the water, respectively.

For the exergy performance, the exergy conversion efficiency ($\eta_{ex,pg}$) can be obtained from the following expression:

Table 3 Standard chemical exergy of selected gases [73].

Substance	Standard Chemical Exergy (kJ/kmol)
Carbon dioxide (CO ₂)	19,870
Carbon monoxide (CO)	275,100
Hydrogen (H_2)	236,100
Methane (CH ₄)	831,650
Nitrogen (N_2)	720
Oxygen (O_2)	3,970
Water vapor (H_2O)	9,500

$$\eta_{ex,pg} = \frac{\dot{E}x_{syngas}}{\dot{E}x_{pw} + \dot{E}x_{Qpreheat,air} + \dot{E}x_{Qpreheat,water} + \frac{P_{torch}}{\eta_{torch}}}$$
(14)

where $\dot{E}x_{syngas}$ is the exergy content of syngas (MW) and $\dot{E}x_{pw}$ is the exergy content of plastic waste (MW), $\dot{E}x_{Q_{preheat,uir}}$ and $\dot{E}x_{Q_{preheat,water}}$ denote the exergy associated with heat transfer for preheating air and water, respectively. It should be noted that the energy and exergy associated with air and water preheating are assumed to be zero when the air and water are internally heated using sensible heat recovered from the raw syngas, such as through integrated heat exchangers.

• Anaerobic digestion

In the first scenario, the energy conversion efficiency ($\eta_{en,ad}$) and exergy conversion efficiency ($\eta_{ex,ad}$) of anaerobic digestion can be mathematically represented as follows:

$$\eta_{en,ad} = \frac{\dot{E}_{biogas}}{\dot{E}_{foodwaste} + \dot{Q}_{AD}}$$
 (15)

$$\eta_{ex,ad} = \frac{\dot{E}x_{biogas}}{\dot{E}x_{foodwaste} + \dot{Q}_{AD} \left(1 - \frac{T_0}{T_{heating}}\right)}$$
(16)

where \dot{E}_{biogas} is energy content of biogas which can be defined using Eq. (7) (MW); $\dot{E}x_{biogas}$ is the exergy content of biogas which can be determined using Eq. (10) (MW); $\dot{E}_{foodwaste}$ is energy content of food waste which can be calculated using Eq. (1) (MW), $\dot{E}x_{foodwaste}$ is exergy content of food waste which can be calculated using Eq. (4) (MW), and \dot{Q}_{AD} is the heating requirement to maintain the digester temperature (38°C).

In the context of Scenario 2, it is important to note that the installation of a water scrubber after the AD requires the involvement of two compressors for biogas purification. As a result, the above energy conversion efficiency of the AD ($\eta_{en,ad}$) and exergy conversion efficiency ($\eta_{ex,ad}$) equation are modified as follows:

$$\eta_{en,ad} = \frac{\dot{E}_{biogas}}{\dot{W}_{comp,ws} + \dot{W}_{pump,ws} + \dot{E}_{fw} + \dot{Q}_{AD}}$$
(17)

$$\eta_{ex,ad} = \frac{\dot{E}x_{biogas}}{\dot{W}_{comp,ws} + \dot{W}_{pump,ws} + \dot{E}x_{fw} + \dot{Q}_{AD} \left(1 - \frac{T_0}{T_{heating}}\right)}$$
(18)

where $\dot{W}_{comp,ws}$, is compressor work (MW) in the water scrubber and $\dot{W}_{pump,ws}$ is pump work (MW) in the water scrubber.

• Gas-turbine power generation

The thermal energy efficiency of the gas-turbine power plant $(\eta_{en,gt})$ and thermal exergy efficiency $(\eta_{ex,gt})$ can be expressed as follows:

For Scenario 1,

$$\eta_{en,gt} = \frac{\dot{W}_{gt} - \dot{W}_{air\ comp,gt} - \dot{W}_{fuel\ comp,gt}}{\dot{E}_{syngas} + \dot{E}_{biogas}}$$
(19)

$$\eta_{ex,gt} = \frac{\dot{W}_{gt} - \dot{W}_{air\ comp,gt} - \dot{W}_{fuel\ comp,gt}}{\dot{E}x_{syngas} + \dot{E}x_{biogas}}$$
(20)

For Scenario 2,

$$\eta_{en,gt} = \frac{\dot{W}_{gt} - \dot{W}_{air\ comp,gt} - \dot{W}_{fuel\ comp,gt}}{\dot{E}_{syngas}} \tag{21}$$

$$\eta_{ex,gt} = \frac{\dot{W}_{gt} - \dot{W}_{air} comp.gt - \dot{W}_{fuel} comp.gt}{\dot{E} \mathbf{X}_{\text{compars}}}$$
(22)

where \dot{W}_{gt} is the gas turbine work (MW), $\dot{W}_{air\ comp,gt}$ is the air compressor work (MW), $\dot{W}_{fuel\ comp,gt}$ is the fuel compressor work (MW).

• Steam-turbine power generation

The thermal energy efficiency of the steam-turbine power plant $(\eta_{en.st})$ and thermal exergy efficiency $(\eta_{ex.st})$ can be formulated as follows:

$$\eta_{en,st} = \frac{\dot{W}_{hpt} + \dot{W}_{ipt} + \dot{W}_{ipt} - (\dot{W}_{hpp} + \dot{W}_{ipp} + \dot{W}_{lpp})}{\dot{Q}_{fluegas}}$$
(23)

$$\eta_{ex,st} = \frac{\dot{W}_{hpt} + \dot{W}_{ipt} + \dot{W}_{lpt} - \left(\dot{W}_{hpp} + \dot{W}_{ipp} + \dot{W}_{lpp}\right)}{\dot{Q}_{fluegas} \left(1 - \frac{T_0}{T_{fluegas}}\right)}$$
(24)

where \dot{W}_{hpt} , \dot{W}_{ipt} , \dot{W}_{lpt} are the high-pressure, intermediate-pressure, low-pressure turbine work (MW), respectively, and \dot{W}_{hpp} , \dot{W}_{lpp} , \dot{W}_{lpp} are the high-pressure, intermediate-pressure, low-pressure pump work (MW), respectively.

• Absorption refrigeration cooling

The energetic coefficient of performance of the ARC ($COP_{en,arc}$) and exergetic coefficient of performance ($COP_{ex,arc}$) can be determined by the following mathematical expression:

$$COP_{en,arc} = \frac{\dot{Q}_{eva}}{\dot{W}_{pump,arc} + \dot{Q}_{gen}}$$
 (25)

$$COP_{ex,arc} = \frac{\dot{Q}_{eva} \left(\frac{T_0}{T_{eva}} - 1\right)}{\dot{W}_{pump,arc} + \dot{Q}_{gen} \left(1 - \frac{T_0}{T_{gen}}\right)}$$
(26)

where $\dot{W}_{pump,arc}$ is the pump work (MW), \dot{Q}_{gen} and T_{gen} are the heat absorbed by the generator (heat released from flue gas) (MW) and its associated temperature (K), respectively, and \dot{Q}_{eva} and T_{eva} are the heat absorbed by the evaporator (heat released from residence house) (MW) and its associated temperature (K), respectively.

• Methane liquefaction

The calculation of the energetic coefficient of performance of the ML $(COP_{en,ml})$ and exergetic coefficient of performance $(COP_{ex,ml})$ can be derived using the subsequent equation:

$$COP_{en,ml} = \frac{\dot{Q}_{refg}}{\dot{W}_{comp,ml}} \tag{27}$$

$$COP_{ex,ml} = \frac{\dot{Q}_{refg} \left(\frac{T_0}{T_{refg}} - 1 \right)}{\dot{W}_{comm,ml}}$$
(28)

where $\dot{W}_{comp,ml}$ is the compressor work (MW), \dot{Q}_{refg} and T_{refg} are the heat required to liquify CH₄ and its associated temperature (K), respectively.

· Overall system

In the first scenario, the system output comprises of electricity, cooling, and heating. Therefore, in order to assess the performance of the overall system in Scenario 1, the energy and exergy efficiency of the system as a whole is defined as follows:

$$\eta_{en,overall,sc1,x} = \frac{\dot{W}_{net,x} + \dot{Q}_{cooling} + \dot{Q}_{heating}}{\dot{E}_{nw} + \dot{E}_{fw}}$$
(29)

$$\eta_{ex,overall,sc1,x} = \frac{\dot{W}_{net,x} + \dot{E}x_{cooling} + \dot{E}x_{heating}}{\dot{E}x_{pw} + \dot{E}x_{fw}}$$
(30)

where:

$$x = baseline, pre - ccs, post - ccs$$
 (31)

$$\dot{W}_{net,baseline} = \dot{W}_{gross,ccgt,baseline} - \left(\dot{W}_{waste\ treatment} + \frac{P_{torch}}{\eta_{torch}}\right)_{pg} - \dot{W}_{pump,arc,baseline}$$
(32)

$$\dot{W}_{net.pre-ccs} = \dot{W}_{gross,ccgt.pre-ccs} - \left(\dot{W}_{waste\ treatment} + \frac{P_{torch}}{\eta_{torch}}\right)_{pg} - \dot{W}_{pump,arc.pre-ccs} - \left(\dot{W}_{pump} + \dot{W}_{comp}\right)_{ccs.pre-ccs}$$

$$\dot{W}_{net,post-ccs} = \dot{W}_{gross,ccgt,post-ccs} - \left(\dot{W}_{waste treatment} + \frac{P_{torch}}{\eta_{torch}}\right)_{pg} - \dot{W}_{pump,arc,post-ccs} - \left(\dot{W}_{pump} + \dot{W}_{comp}\right)_{ccs,post-ccs}$$

$$(34)$$

where $\dot{W}_{net,baseline}$, $\dot{W}_{net,pre-ccs}$, $\dot{W}_{net,post-ccs}$ are the net work (MW) in baseline, case with pre CCS, case with post CCS, respectively; $\dot{Q}_{cooling}$ and $\dot{E}x_{cooling}$ are the cooling energy and exergy generated from the ARC (MW), respectively; $\dot{Q}_{heating}$ and $\dot{E}x_{heating}$ are the heating energy and exergy released from the system (MW), respectively; $\dot{W}_{gross,ccgt}$ is the gross power generated from the CCGT (MW); $\dot{W}_{waste\ treatment}$ is the power required for crushing the plastic waste (MW); \dot{W}_{torch} is the plasma torch power (MW); $\dot{W}_{pump,arc}$ and $\dot{W}_{pump,ccs}$ are the pump power in the ARC and in the CCS plant (MW), respectively; $\dot{W}_{comp,ccs}$ is the compressor power in the CCS plant (MW).

In Scenario 2, the output consists of power, cooling, heating, and liquid fuel. Hence, in order to evaluate the performance of the entire system in Scenario 2, the energy and exergy efficiency of the total system can be determined in the following formula:

$$\eta_{en,overall,sc2,x} = \frac{\dot{W}_{net,x} + \dot{E}_{CH4\ liq} + \dot{Q}_{cooling} + \dot{Q}_{heating}}{\dot{E}_{pw} + \dot{E}_{fw}}$$
(35)

$$\eta_{ex,overall,sc2,x} = \frac{\dot{W}_{net,x} + \dot{E}x_{CH_4 \ liq} + \dot{E}x_{cooling} + \dot{E}x_{heating}}{\dot{E}x_{pw} + \dot{E}x_{fw}}$$
(36)

where:

$$x = baseline, pre - ccs, post - ccs$$
 (37)

$$\dot{W}_{net,baseline} = \dot{W}_{gross,ccgt,baseline} - \left(\dot{W}_{waste\ treatment} + \frac{P_{torch}}{\eta_{torch}}\right)_{pg} - \dot{W}_{pump,arc,baseline} - \left(\dot{W}_{pump} + \dot{W}_{comp}\right)_{ws} - \dot{W}_{comp,ml}$$
(38)

$$\dot{W}_{net.pre-ccs} = \dot{W}_{gross,ccgt.pre-ccs} - \left(\dot{W}_{waste\ treatment} + \frac{P_{torch}}{\eta_{torch}}\right)_{pg} - \dot{W}_{pump,arc.pre-ccs} - \left(\dot{W}_{pump} + \dot{W}_{comp}\right)_{ws} - \dot{W}_{comp,ml} - \left(\dot{W}_{pump} + \dot{W}_{comp}\right)_{ccs.pre-ccs}$$

$$(39)$$

$$\dot{W}_{net,post-ccs} = \dot{W}_{gross,ccgt,post-ccs} - \left(\dot{W}_{waste\ treatment} + rac{P_{torch}}{\eta_{torch}}
ight)_{pg} - \dot{W}_{pump,arc,post-ccs} - \left(\dot{W}_{pump} + \dot{W}_{comp}
ight)_{ws} - \dot{W}_{comp,ml} - \left(\dot{W}_{pump} + \dot{W}_{comp}
ight)_{ccs,post-ccs}$$

where $\dot{E}_{CH_4 \ liq}$ and $\dot{E}_{XCH_4 \ liq}$ are the energy and exergy content of liquid biomethane (MW), respectively; $\dot{W}_{pump,ws}$ and $\dot{W}_{comp,ws}$ are the pump and compressor power in the WS (MW), respectively; $\dot{W}_{comp,ml}$ is the compressor power in the ML (MW).

2.4. Limitation of the study

The waste utilization process presented in this study offers a promising pathway for waste management, particularly in waste reduction and valuable energy generation. However, as with any emerging technology, certain limitations remain. A key challenge lies in translating numerical results into real-world implementation. One major factor is the integration of these processes into existing industrial infrastructure to ensure operational feasibility and efficiency. Additionally, it is crucial to establish a reliable transport and storage system for captured carbon dioxide to support the practical deployment of carbon capture technologies.

While this study applies energy and exergy analysis to evaluate the thermodynamic performance of a novel waste-to-energy system, it is important to recognise that exergy analysis can also serve a broader theoretical framework, which encompasses economic, environmental, and social dimensions. The literature shows the application of this extended exergy accounting (EEA) approach to evaluate sustainability criteria. For instance, Liu et al. [75] applied EEA to evaluate food waste treatment strategies in Singapore, and identified anaerobic digestion as the most sustainable option in terms of urban ecosystem costs and revenues in addition to energy efficiency. Similarly, Liu et al. [76] developed an EEA based multi criteria decision making framework to optimize the waste to energy facility locations under uncertainty by integrating material, energy, labour, capital, and environmental factors into a single exergy-based model. Hendo and Sanaye [77] further demonstrated the value of integrating economic and exergy analysis through simultaneous multi objective optimization, which showed that such an approach can significantly reduce payback periods and improve system efficiency when applied to incineration plants.

Although the current study is limited to thermodynamic analysis, future work will include techno-economic and LCA. Specifically, the economic analysis will quantify capital and operational expenditures and estimate the levelized cost of energy and products. The LCA will evaluate the system's environmental impacts across its lifecycle. Together, these methods will support a more comprehensive understanding of the system's practicality, cost-effectiveness, and long-term sustainability.

3. Results and discussion

3.1. Model validation

Table 4 presents a comparison between the modelling results of PG, AD, GT power cycle, ST power cycle and ML and their related experimental data. Based on these findings, it can be concluded that there is a good agreement between the results derived from the current model and relevant experimental data.

3.2. Energy and exergy performance

3.2.1. Syngas and biogas generation

In order to generate syngas using a PG, an ER of 0.14, a SAMR of 0.396, and a SFR of 0.8 are employed to attain a temperature of 2500° C

Table 4Comparison between the simulation outcomes of the present study with results of previous studies.

Process	Parameter	Present work	Experimental	References
PG	H ₂ (mol %)	62.03	57	[78]
	CO (mol %)	18.44	18.8	
	CO ₂ (mol %)	19.28	15.7	
	Plasma torch power (MW)	34.34	27.2	
AD	CH ₄ (mol %)	38.7	37.4	[61]
	CO ₂ (mol %)	60.5	62.6	
	Specific biogas yield (m³/tonnes VS)	605.27	642	
	Specific methane yield (m³/tonnes VS)	366.19	402	
	Digestate (kg/s)	1080.89	1113.42	
GT power cycle	Compressor Power (MW)	214.35	215.79	[66]
	Turbine Power (MW)	430.89	430.28	
	Turbine Outlet Temperature (°C)	603.28	604	
ST power cycle	Total steam turbine power (MW)	242.4	232.97	[66]
	Pump power (MW)	3.66	3.37	
	Turbine Outlet Temperature (°C)	34.94	32.25	
ML	Liquefaction temperature (°C)	-152.698	-161.5	[69]
	COPactual	0.26	0.23	

in the HTZ. The amount of plasma torch power used in the current PG is around 40.04 MW. Steam is generated at a high temperature of approximately 1157°C by harnessing the heat from the raw syngas. The process flow diagram of the PG for baseline case, the case with pre-CCS and the case with post CCS can be seen in Figs. S.1–S.3 in the **Supplementary Information**, respectively.

Table 5 presents the mass flow rates of the feedstock and the generated gas, along with their energy and exergy content, fuel gas composition, and the performance parameters of the PG and AD. The mass flow rates of plastic waste (PW) and food waste (FW) are derived from the amounts received at the Benowo landfill [1]. As shown in the Table 5, the primary components of the raw syngas are predominantly $\rm H_2$ at 43%, followed by nitrogen $\rm N_2$ at 25%, and CO at 24%. In

Table 5Material and energy balances for the PG and AD systems.

Characteristic Feed stock			Generated	gas		Unit
	Plastic waste	Food waste	Raw syngas	Raw biogas	Syngas after pre- CC	
Mass flow rate	5.00	13.97	18.45	3.31	10.04	kg/s
Energy content	184.11	45.67	191.85	44.26	163.09	MW
Exergy content	193.11	53.37	184.08	48.21	157.67	MW
Composition of	fuel (molar	fraction)				
H_2	N/A	N/A	42.56	0.00	67.24	%
CO	N/A	N/A	24.01	0.00	1.73	%
CH_4	N/A	N/A	0.00	47.50	0.00	%
N_2	N/A	N/A	25.09	0.00	25.98	%
H ₂ O	N/A	N/A	6.93	5.20	3.92	%
CO_2	N/A	N/A	1.40	43.40	1.14	%
O_2	N/A	N/A	0.00	0.00	0.00	%
NH ₃	N/A	N/A	0.00	3.60	0.00	%
H_2S	N/A	N/A	0.00	0.40	0.00	%
Performance pa	rameter	Plasma g	asifier	Anaerobi	c digester	Unit
Energy conversion	on	75.28		88.34	-	%
Exergy conversion efficiency	on	70.75		86.28		%

comparison with the results obtained by Zhang et al. [79] who used the same type of gasifier and gasification agents (air and steam), the results of the current study demonstrate higher energy and exergy efficiency. Specifically, the energy and exergy efficiency of the PG in the reference study are 50.8% and 44.9%, while the current study achieved 75.28% and 70.75%, respectively. This is a result of the higher carbon and hydrogen content of the feedstock utilized, i.e. waste plastic compared to the solid waste utilized in [79], 79.77% vs 50.5% and 15.47% vs 5.6%, respectively which results in higher LHV for the plastic waste.

For the pre-CCS cases, the syngas produced by the PG reacts with steam in the WGS reactor. This reaction results in the generation of CO2 and hence its composition is further increased in the syngas, which is then captured in the CCS plant. A 10% portion of the raw syngas has to be combusted to raise heat for steam generation. By optimizing the AFR to a value of 15.69, it is possible to attain the highest temperature of the combustion gas, which is around 633°C. The highest possible conversion of CO into CO₂ and H₂ that can be attained is ~93% by employing a steam to carbon monoxide molar ratio (S/C ratio) of 1.66. Due to the conversion in the WGS reactor, the mass flow rate of CO reduces dramatically from 7.53 to 0.47 kg/s, while there is an increase in the mass flow rate of hydrogen H₂ from 0.961 to 1.318 kg/s. After the syngas passes through the WGS reactor and pre-CCS plant, there is a reduction in the energy and exergy content of the syngas, as shown in the Table 5. The process flow diagram of WGS reactor is shown in Fig. S.4 in the Supplementary Information.

For biogas generation, in order to maintain the temperature of the AD at 38°C, approximately 10% of the energy content of the biogas, equivalent to 4.42 MW, is required. The heating requirement can be satisfied by extracting 0.83 MW of energy from the flue gas after passing through the ARC, and an additional 3.59 MW from the sensible heat of the raw syngas (for the baseline scenario) or from extracting heat from the top stream of the desorber prior to the condenser (for the case with pre- and post-CCS). The energy conversion efficiency of the AD process can be observed in Table 5, with values of around 88.34%. According to [80], the conversion of food waste into biogas has an energy efficiency of approximately 85%, which is in good agreement with the energy efficiency of 88.34% calculated herein.

3.2.2. Electricity generation

Table 6 contains detailed information about the performance of the CCGT under different scenarios and configurations. Key parameters analyzed include fuel energy input, compressor power consumption,

turbine power output, and performance efficiency. It can be seen from this table that the energy input to the GT power cycle remains the same in the baseline case and the case with post-CCS in both scenarios. Nevertheless, the energy content of fuel in the case with pre-CCS is always lower than in the other cases. There are two primary factors contributing to this phenomenon. Firstly, the mass flow rate of CO decreases significantly and the rise of the mass flow rate of H_2 is not enough to offset this. Secondly, 10% of the raw syngas is extracted to supply heat in the WGSR. The higher energy of fuel on scenario 1 compared to scenario 2 is attributed to the mixture of syngas and biogas used in the combustor of scenario 1, whereas only syngas is utilized in the combustor of scenario 2.

According to Table 6, the baseline case and the case with post-CCS in Scenario 1 and 2 generate higher amounts of CCGT fuel, resulting in a bigger amount of air being drawn into the compressor and consequently a higher air compressor power compared to the case with pre-CCS is required. Given that all the cases have the same turbine inlet temperature, the only variable that impacts the turbine work is the combined mass flow rate of air and fuel. Therefore, the baseline case and the post-CCS case can generate more electricity in the GT compared to the pre-

The flue gas from the GT power cycle is utilized to drive a typical steam turbine (ST) cycle. The amount of heat that can be recovered by the boiler feed water (BFW) depends on the temperature at which it enters the heat recovery steam generator (HRSG). In the baseline case, the BFW is condensate water that comes out from the LP pump (stream 8, as shown in Fig. S.6, **Supplementary Information**) and absorbs most of the available heat. The BFW temperature in the baseline case for Scenarios 1 and 2 is 35°C.

While the baseline case benefits from the lower temperature of the BFW, allowing for greater heat absorption, the situation changes in the pre- and post-CCS cases. The energy absorbed from the flue gas by the BFW (stream 8, as shown in Fig. S.7, **Supplementary Information**) is reduced because the BFW has been preheated using sensible heat from the desuperheater. Specifically, the temperature of BFW before entering the HRSG in the case with pre-CCS for Scenarios 1 and 2 is 82°C and 80°C, respectively. In the post-CCS case, the BFW temperature rises to 143°C and 119°C for Scenarios 1 and 2, respectively. Additionally, it is noteworthy that the lowest amount of energy delivered to the HRSG through the flue gas in the pre-CCS case is due to the lowest fuel energy.

Finally, the net power output of the combined cycle is maximum in the baseline case because it has a higher flow rate of fuel, and the

Table 6Thermodynamic results for the CCGT island.

Parameter	SCENARIO 1			SCENARIO 2	SCENARIO 2		
	BASELINE	W/PRE-CCS	W/POST-CCS	BASELINE	W/PRE-CCS	W/POST-CCS	
Gas turbine performance							
Energy of fuel (to the gas turbine cycle)	236.11	207.32	236.11	191.85	163.09	191.85	MW
Exergy of fuel (to the gas turbine cycle)	231.48	195.30	231.48	184.08	157.67	184.08	MW
Air compressor power in the gas turbine cycle	89.51	81.06	89.51	72.03	62.15	72.03	MW
Fuel compressor power in the gas turbine cycle	15.72	13.33	15.72	14.29	12.55	14.29	MW
Gross gas turbine power	186.03	166.53	186.03	150.61	129.97	150.61	MW
Net power output from GT cycle	80.79	72.14	80.79	64.29	55.27	64.29	MW
Thermal energy efficiency	34.22	34.80	34.22	33.51	33.89	33.51	%
Thermal exergy efficiency	34.90	36.94	34.90	34.92	35.05	34.92	%
Steam turbine performance							
Energy of flue gas (to the steam turbine cycle)	123.48	107.70	115.88	99.42	83.72	96.77	MW
Exergy of flue gas (to the steam turbine cycle)	63.02	54.68	61.20	50.68	42.49	50.06	MW
Pump power in the steam turbine cycle	0.84	0.78	0.89	0.70	0.63	0.74	MW
Steam turbine power	51.11	39.18	37.74	41.61	30.94	32.23	MW
Net power output from ST cycle	50.27	38.40	36.85	40.91	30.31	31.50	MW
Thermal energy efficiency	40.71	35.66	31.80	41.15	36.21	32.55	%
Thermal exergy efficiency	79.77	70.23	60.21	80.72	71.33	62.91	%
Overall combined cycle performance							
Net power output from CCGT	131.06	110.54	117.64	105.20	85.58	95.78	MW
CCGT energy efficiency	55.51	53.32	49.83	54.83	52.47	49.93	%
CCGT exergy efficiency	56.62	56.60	50.82	57.15	54.28	52.03	%

absence of LP steam necessary for the CCS to meet the reboiler heat duty. This extraction reduces the net power generated by the steam turbine in both CCS cases. Specifically, as shown in Table 6, the net power output in the baseline case for Scenarios 1 and 2 is 131.06 MW and 105.20 MW, respectively. In contrast, the post-CCS case, which maintains the same fuel flow rate as the baseline but includes LP steam extraction, shows the second-highest net power output. The net power output for post-CCS in Scenarios 1 and 2 is 117.46 MW and 95.78 MW, respectively, with heat supplies of 58.33 MW and 41.81 MW of thermal energy to the CCS plant. The lowest net power output is observed in the pre-CCS case, with outputs of 110.54 MW and 85.58 MW for Scenarios 1 and 2, respectively, and corresponding heat supplies of 43.63 MW and 35.58 MW for the CCS plant.

3.2.3. Cooling and heating generation

The process flow diagram of the ARC is provided in **Section S.1.5 of Supplementary Information.** Table 7 compares various system operating conditions and presents the corresponding energy and exergy analyses for ARC. As shown, the post-CCS case in both scenarios exhibits the highest flue gas temperature due to the limitation in the HRSG (temperature crossover between the flue gas and the incoming BFW).

Additionally, Table 7 indicates that the cooling capacity is identical in both the baseline and post-CCS cases under both scenarios, but these are higher than in the pre-CCS case. Since the temperature difference is fixed during the operation of the evaporator, the only remaining factor determining the cooling effect produced by the ARC is the mass flow rate of the ARC working fluid. While the ratio of the mass flow rates of ARC working fluid and flue gas is 1:10 (as listed in Table 1), the flow rate of flue gas in each case is the determining factor of the cooling capacity. This explains the difference between the baseline and the post-CCS cases vs the pre-CCS case (4.04 vs 3.51 MW in Scenario 1 and 3.27 vs 2.72 MW in Scenario 2).

The amount of heat energy recovered from the ARC is presented in Table 7. As shown, the pre-CCS case recovers the highest amount of heat energy due to the highest heating air flow rate. The heating air flow rate is iteratively adjusted until the heating air temperature reaches 52°C. However, in terms of heat exergy recovery, the post-CCS case exhibits the highest value, as the temperature of the recovered heat from the flue gas is higher.

As presented in the Table 7, the energy COP of the ARC is consistent across all scenarios, with a value of around 0.74. This result aligns with previous research findings, where the COP was reported as 0.75 in [81] and 0.74 in [82]. The exergy COP in both Scenario 1 and Scenario 2 ranges between 0.22 and 0.28, which is comparable to the COP range of 0.2 to 0.25 identified in [83]. The exergy COP in the case with post-CCS

under both scenarios is consistently lower compared to the baseline and pre-CCS cases due to higher heat loss during the heat transfer from the flue gas to the ARC working fluid in the desorber. The higher heat loss is due to the ratio established between the ARC working fluid and flue gas flow rates through the desorber.

3.2.4. Liquid biomethane production

Biogas at a flowrate of 3.31~kg/s with CO_2 and CH_4 molar fractions of 43.3% and 47.4%, respectively, is upgraded to 97.7% CH4 using a HPWS process operating at 10~bar and $25^{\circ}C$. The integration of HPWS with the anaerobic digester results in a slight reduction in both energy and exergy efficiency, from 88.34% to 85.79% and from 86.28% to 84.04%, respectively. This decrease is primarily attributed to the energy consumption required for biogas compression and water pumping within the HPWS.

In the subsequent methane liquefaction (ML) process, 5.24 MW of power is required to compress the upgraded biomethane to 200 bar. The energy COP for the ML process is 0.29, which is consistent with previous studies, such as the research cited in [69], where a COP of approximately 0.234 was reported.

3.2.5. CCS plant

Table 8 compares several critical parameters between pre-CCS and post-CCS across two scenarios. Parameters such as liquid-to-gas (L/G) ratio, specific reboiler duty (SRD), and reboiler heat duty are examined to evaluate the performance of the carbon capture processes. Modelling approach and other important parameters such as the dimension of absorber and stripper, lean solvent loading (LSL), rich solvent loading

Table 8
Main input and results for the pre- and post-CCS plant.

Parameter	Pre-CCS		Post-CCS	Unit	
	Scenario 1	Scenario 2	Scenario 1	Scenario 2	
Gas input flow rate	23.83	20.61	205.12	165.89	kg/s
Absorber height	25	25	25	25	m
Absorber diameter	5	4	8.5	7.5	m
CO ₂ concentration in gas input	53.52	51.10	8.37	7.54	% (mass)
CO ₂ captured flow rate	12.16	10.05	16.33	11.94	kg/s
L/G ratio	5.45	5.28	0.88	0.80	kg/kg
Reboiler heat duty	40.29	34.30	58.18	43.05	MW
SRD	3.31	3.41	3.56	3.60	GJ/
					tCO_2

Table 7Results for the absorption refrigeration cooler (ARC).

Parameter	SCENARIO 1		SCENARIO 2			UNIT	
	Baseline		W/POST-CCS	Baseline	W/PRE-CCS	W/POST-CCS	
Operating condition							
Flue gas temperature	110.00	110.00	144.24	110.00	110.00	124.78	°C
Pump power	0.12	0.11	0.12	0.10	0.08	0.10	kW
Working fluid flow rate	20.79	18.04	20.79	16.81	13.96	16.81	kg/s
Energy analysis							
Energy of flue gas absorbed by ARC	5.50	4.77	5.50	4.45	3.69	4.45	MW
Cooling energy for residence house	4.04	3.51	4.04	3.27	2.72	3.27	MW
Energy COP	0.74	0.74	0.74	0.74	0.74	0.74	-
Exergy analysis							
Exergy of flue gas absorbed by ARC	1.22	1.06	1.57	0.99	0.82	1.11	MW
Cooling exergy for residence house	0.34	0.29	0.34	0.27	0.23	0.27	MW
Exergy COP	0.28	0.28	0.22	0.28	0.28	0.25	-
Waste heat from ARC*							
Energy of the waste heat	17.29	27.87	26.84	13.99	25.62	17.12	MW
Exergy of the waste heat	1.62	2.83	3.28	1.49	2.70	3.13	MW
Heating air flow rate	631.10	1016.98	948.52	510.48	934.91	624.86	kg/s

^{*} The heat recovered comes from the absorber, condenser, and the waste heat recovery HX

(RSL) as well as the process flow diagram of the CCS plant, are provided in section **S.1.6** of Supplementary Information.

Based on the Table 8, L/G ratio in the case with pre-CCS is higher than that in the case with post-CCS as more CO₂ per cross sectional area has to be captured. The reboiler heat duty in Scenario 1 is consistently higher than in Scenario 2 due to the greater amount of carbon captured in the first scenario. Specifically, in the pre-CCS case, the CCS plant in Scenario 1 captures 18.90 kg/s of carbon, compared to 14.59 kg/s in Scenario 2. Similarly, in the post-CCS case, the CCS plant in Scenario 1 captures 24.69 kg/s, while Scenario 2 captures 17.89 kg/s. Further, the pre-CCS cases exhibit lowers SRDs compared to the post-CCS, i.e. 3.31 and 3.41 GJ/tCO2 (for Scenario 1 and 2) vs 3.56 and 3.6 GJ/tCO2 (Scenario 1 and 2), respectively, due to the higher concentrations of ${\rm CO_2}$ in the treated gas. Interestingly, despite the differences in captured carbon, the SRD shows minimal variation across the cases, ranging from 3.31 GJ/tCO₂ to 3.6 GJ/tCO₂. These results align with findings from [84, 85], which indicate that with a LSL of 0.11-0.12 mol CO₂/mol MEA and an absorption packing height of 24 m, the SRD is approximately 3.5 GJ/tCO₂.

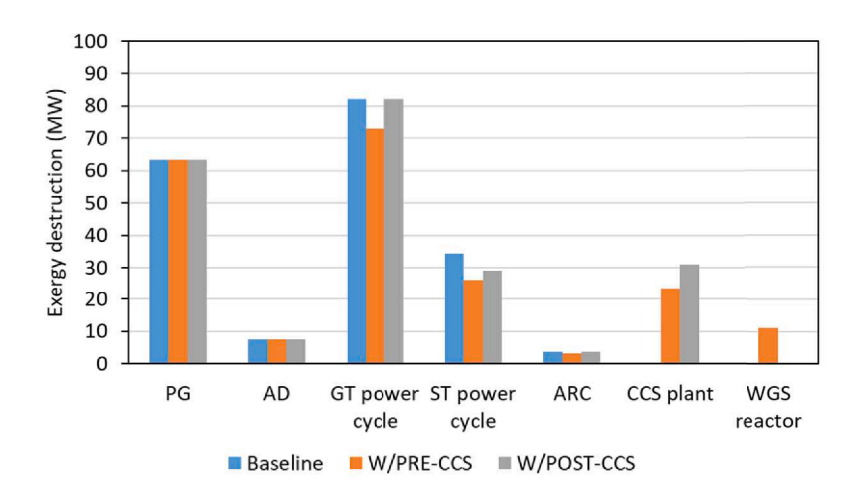
3.3. Exergy destruction

Fig. 3 illustrates the distribution of exergy destruction across various

subsystems of the scenarios and configurations explained above. The graphs highlight the differences in inefficiencies among the subsystems, offering insights into where exergy losses occur and where improvements could be made to enhance overall system efficiency. The detail exergy destruction of each component can be seen in the **Supplementary** Information **Section S.2**.

As seen in Fig. 3, the PG and the GT power cycle have the highest exergy destruction across all plant scenarios. The PG has an exergy destruction rate of 63.37 MW, primarily due to the irreversibility associated with the high gasification temperature caused by the plasma torch and the chemical reactions taking place for converting the plastic waste into high temperature of syngas and slag [25,86,87]. In the GT power cycle, the exergy destruction spans from 58 MW to 83 MW, with the combustion chamber (CC) being the largest contributor. This loss is caused by the irreversibility of the oxidation reactions of the fuel gas to produce thermal energy [88].

In addition to the PG and GT power cycle, the exergy destruction within the ST power cycle ranges from 20 to 35 MW. The HRSG, steam turbine, and condenser accounted for the majority of exergy destruction in this subsystem. The exergy destruction in the HRSG is mostly affected by heat transfer irreversibility between the exhaust gases and the steam. Meanwhile, the exergy destruction of the steam turbine is caused by expansions at high pressure and temperature across multiple stages.



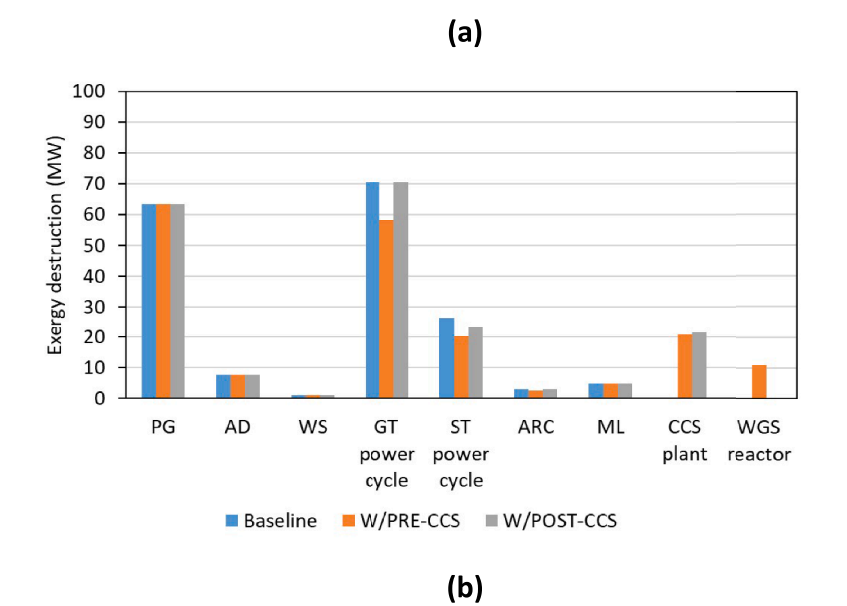


Fig. 3. Exergy destruction of each energy subsystem in (a) Scenario 1 (b) Scenario 2.

Finally, the exergy destroyed in the condenser results from heat loss as the expanded LP steam exiting the LP turbine is cooled down by the cooling water, which is at a low temperature of 25°C [89].

Moreover, the carbon capture facility exhibits significant exergy destruction, varying from 20 MW to 31 MW, with the stripper being the primary source. The exergy loss is caused due to the heating of the solvent to release the absorbed CO_2 using LP steam, the chemical reaction that occurs during the desorption process, and the pressure drops experienced by the solutions as they flow through the stripper [90–92].

Finally, the WGS reactor demonstrates an exergy destruction of approximately 11 MW. The disparity in temperature between the reactants and products leads to significant exergy degradation. The WGS reactor in this study operates at two distinct temperatures: a high-temperature shift of $450^{\circ}\mathrm{C}$ and a low-temperature shift of $200^{\circ}\mathrm{C}$. Other components, such as AD, ARC, ML, and WS, have an exergy destruction below 10 MW. The processes on these sub systems operate under low-temperature conditions, leading to lower exergy destruction compared to high-temperature chemical reactions.

3.4. Carbon balance

Figs. 4 and 5 illustrate the carbon mole flow in both Scenario 1 and

Scenario 2, showing how carbon distribution changes depending on whether the system operates under baseline, pre-CCS, or post-CCS configurations. As shown, CO_2 emissions are higher in all three configurations of Scenario 1 compared to Scenario 2. This is because Scenario 1 releases more flue gas due to the combustion of both syngas and biogas in the gas turbine power plant, whereas in Scenario 2, only syngas is combusted, and the biogas is converted into liquid biomethane. In Scenario 1, the flue gas contains both biogenic and fossil carbon, while in Scenario 2, the flue gas consists only of fossil carbon.

The baseline case in each scenario emits the highest amount of carbon due to the absence of CCS integration. In Scenario 1, the baseline case emits 0.247 kgCO $_2$ released per kg of waste processed, and in Scenario 2, the emission factor is 0.213 kgCO $_2$ per kg of waste processed.

In the pre-CCS configuration, CO_2 emissions are higher than in the post-CCS case. This occurs because, prior to entering the pre-CCS plant, not all CO in the syngas can be fully converted into CO_2 inside the WGS reactor. As a result, the combustion of CO still releases amounts of CO_2 into the atmosphere. As shown in Figs. 4b & 5b, the CO_2 emissions in the pre-CCS case are $0.072 \text{ kg}CO_2$ per kg of waste processed in Scenario 1 and $0.068 \text{ kg}CO_2$ released per kg of waste processed in Scenario 2.

In contrast, in the post-CCS case, the capture process occurs after the conversion of all carbon in the fuel to CO₂, resulting in a more direct and

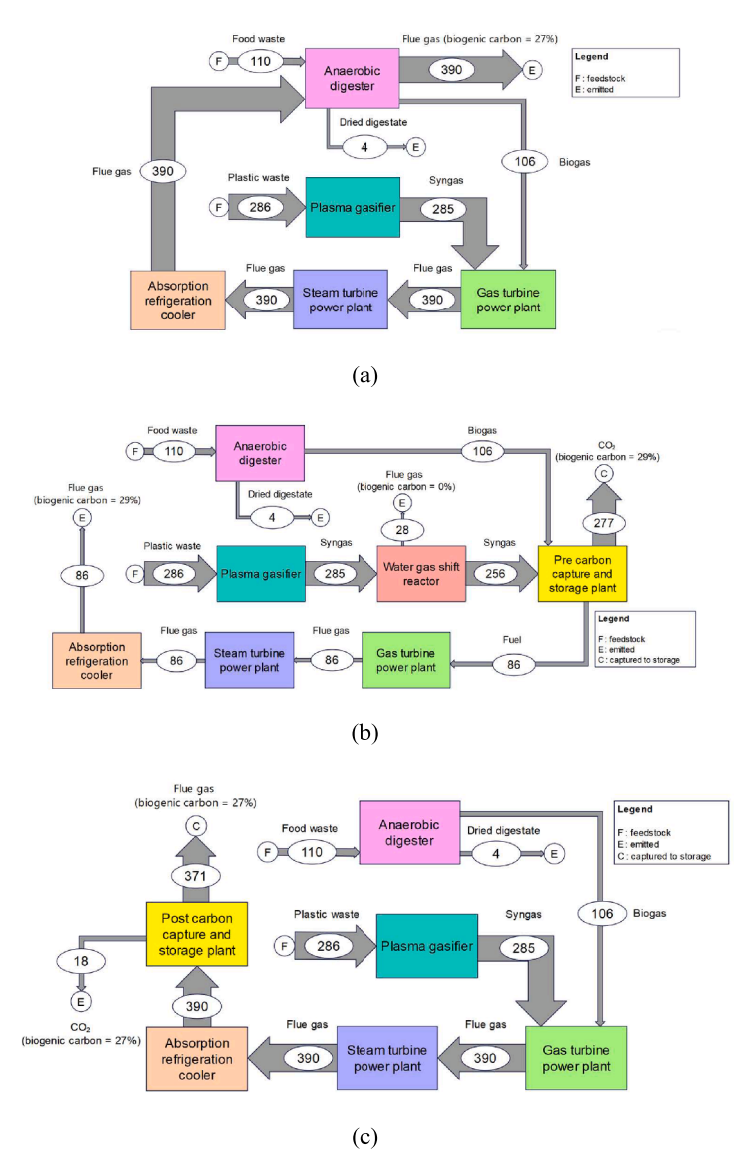


Fig. 4. Carbon mole flow (kmol/s) for Scenario 1: (a) baseline, (b) pre-CCS, (c) post-CCS.

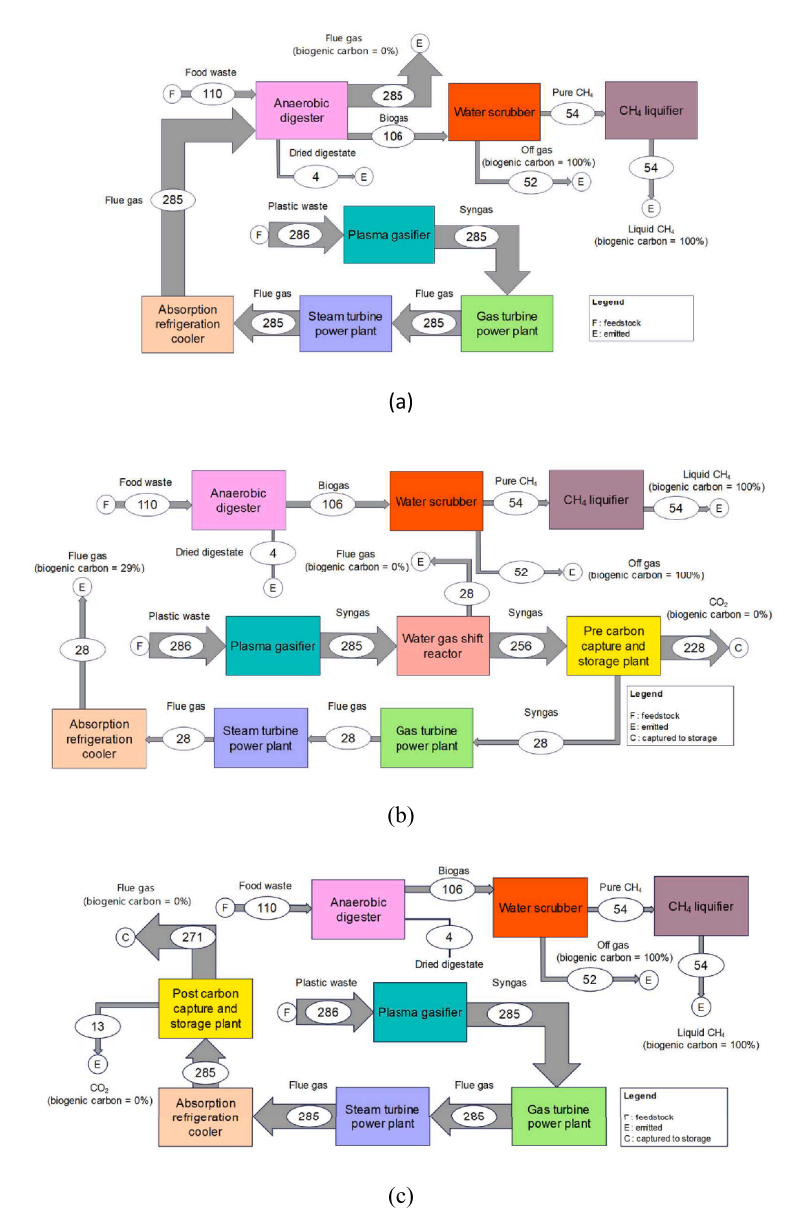


Fig. 5. Carbon mole flow (kmol/s) in Scenario 2: (a) baseline, (b) pre-CCS, (c) post-CCS.

efficient capture of the generated carbon. The case with post-CCS plant emits the least $\rm CO_2$, around $0.011~kg\rm CO_2$ released per kg of waste processed and $0.008~kg\rm CO_2$ released per kg of waste processed for Scenario 1 and 2, respectively.

3.5. Electricity distribution

The electricity generated by the CCGT is used to power the various components within the system. Fig. 6 illustrates the distribution of electricity consumption across the system for both Scenario 1 and Scenario 2 under three different configurations. The data highlights how electricity demand varies depending on the type of the components, energy production method and carbon capture technologies.

By comparing the components' operations in each configuration, it is evident that the plasma gasification unit consistently consumes the most electricity, reaching up to 45.39 MW. This high consumption is primarily due to the need for generating and maintaining plasma at extremely high temperatures, which is essential for efficiently breaking down plastic waste.

The energy vectors generated also affect electricity consumption in

each scenario. Scenario 1, which produces electricity, cooling, and heating, has a lower electricity demand compared to Scenario 2, which generates electricity, cooling, heating, and liquid biomethane. In Scenario 1, the mixture of syngas and biogas is used as fuel for the gas turbine (GT) power plant, while Scenario 2 converts biogas into liquid biomethane rather than burning it. The additional steps in Scenario 2, including upgrading biogas into biomethane and the biomethane liquefaction process, lead to higher electricity consumption.

Additionally, the type of carbon capture technology influences electricity consumption within the system. Pre-CCS requires less electricity than post-CCS due to the lower amount of CO_2 captured and sequestered. The highest electricity consumption in both CCS systems is attributed to the operation of compressors, which are needed to increase the input gas pressure to 1.18 bar and raise the pressure of the captured CO_2 to 83 bar. The type of fuel used in the GT power plant also impacts electricity demand in the CCS systems. In Scenario 1, which uses a mixture of biogas and syngas as fuel, the CCS systems consume more electricity compared to Scenario 2, where only syngas is used. This is because more electricity is required to remove the higher CO_2 concentration in the fuel mixture.

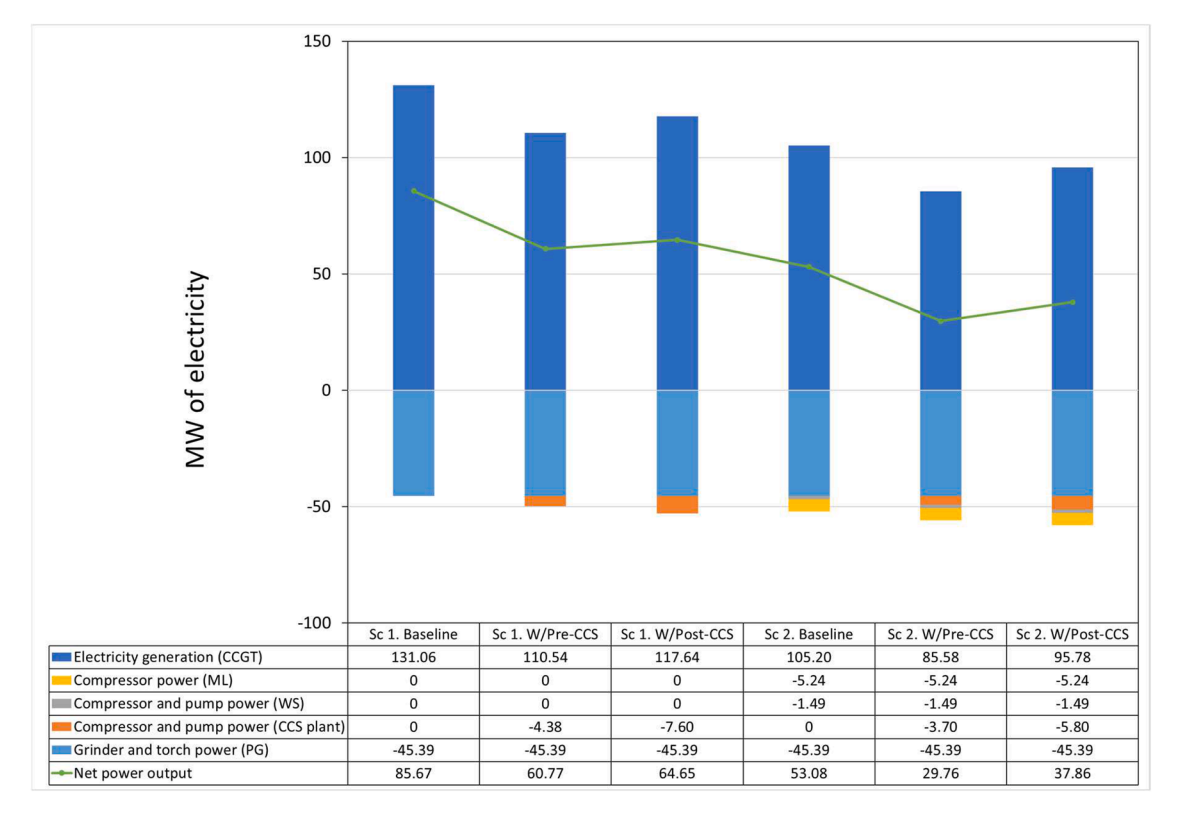


Fig. 6. Electricity generation and consumption breakdown for Scenario 1 and Scenario 2 across the three configurations.

Finally, as shown in Fig. 6, the baseline cases in both scenarios yield the highest net power output due to the combination of maximum electricity generation and minimal electricity consumption. Specifically, in Scenario 1, the net power output reaches 85.67 MW, while in Scenario 2, it is 53.08 MW.

3.6. Overall system performance

Table 9 compares the overall performance of the system in Scenario 1 (electricity, heating, and cooling) and Scenario 2 (electricity, heating, cooling, and liquid biomethane) across three configurations: baseline, pre-CCS, and post-CCS. The key parameters examine include total energy generation, total exergy generation, system energy efficiency, and system exergy efficiency.

As shown in Table 9, Scenario 2 achieves higher system energy and exergy efficiency compared to Scenario 1, despite generating lower levels of power, cooling, and heating. This increased efficiency is mainly attributed to the high efficiency of biomethane production, which has energy and exergy conversion efficiencies of 85.79% and 84.04%,

Table 9Thermodynamic results for the overall system performance for Scenario 1 and Scenario 2.

Overall system performance	Case		UNIT	UNIT	
	Baseline	W/PRE-CCS	W/POST-CCS		
Scenario 1 (electricity, heati	ing, and coo	ling)			
Total energy generation	107.01	92.14	95.54	MW	
Total exergy generation	87.63	63.89	68.27	MW	
System energy efficiency	46.57	40.10	41.58	%	
System exergy efficiency	35.55	25.92	27.70	%	
Scenario 2 (electricity, heati	ing, cooling,	and liquid bion	nethane)		
Total energy generation	113.59	101.36	101.52	MW	
Total exergy generation	101.56	79.41	87.99	MW	
System energy efficiency	49.44	44.11	44.18	%	
System exergy efficiency	41.20	32.22	35.70	%	

respectively, as mentioned in Section 3.2.4. In contrast, the combined-cycle gas turbine (CCGT) has thermal energy efficiency ranging from 49% to 56% and exergy efficiency between 50% and 58%, as shown in Table 6.

The baseline case consistently achieves the highest energy and exergy efficiency in both scenarios, followed by the post-CCS case, with the pre-CCS case showing the lowest efficiencies. The reason is that the baseline case does not provide heat for the stripper in the carbon capture plant and does not allocate 10% of syngas for WGSR. Although the heat demand in the post-CCS case is higher than in the pre-CCS case, the pre-CCS case has less total energy and exergy generation due to the 10% syngas allocation to the WGSR.

Considering both energy production and carbon emissions, the post-CCS case in Scenario 2 emerges as the most favourable option for wasteto-energy utilization. This configuration balances efficient energy production with significant carbon reduction, making it a key solution to adopt low-carbon technologies and mitigate climate change.

4. Conclusion

This study demonstrates the significant potential of integrating waste-to-energy systems with carbon capture and storage (CCS) technologies to address both energy demands and environmental concerns. By utilizing 5 kg/s of plastic waste and 13.97 kg/s of food waste as feedstocks, the research evaluates for the first time the thermodynamic performance of an integrated energy system consisting of a plasma gasifier (PG), anaerobic digester (AD), combined-cycle gas turbine (CCGT), absorption refrigeration cooler (ARC), and biomethane liquefier. Two scenarios, each with three configurations (baseline, pre-CCS, and post-CCS), were explored to assess the system's energy and exergy efficiency, as well as carbon emissions.

The findings of the study indicate that Scenario 1, which is a CCHP system, generated higher amount of electricity, heating and cooling output, but had lower overall efficiency compared to Scenario 2, which includes liquid biomethane production. The baseline case of Scenario 2

achieves the highest overall energy and exergy efficiency, with maximum efficiencies of 49.44% and 41.20%, respectively. On the other hand, the post-CCS configuration of Scenario 2 emits the lowest amount of CO_2 , i.e. $0.008\ kgCO_2$ per kg of waste processed.

These results highlight the effectiveness of integrating advanced waste conversion technologies with CCS in enhancing energy recovery and significantly reducing greenhouse gas emissions. The findings provide a promising pathway for sustainable waste management and energy production, offering valuable insights for detailed engineering studies, policy development, and academic research. Future research will focus on conducting economic and life cycle assessments for both Scenarios 1 and 2 to further evaluate their feasibility and sustainability.

CRediT authorship contribution statement

Qurrotin Ayunina Maulida Okta Arifianti: Writing – original draft, Validation, Software, Methodology, Investigation, Formal analysis, Conceptualization. Stavros Michailos: Writing – review & editing, Validation, Software, Methodology, Investigation, Formal analysis, Conceptualization. Maria Fernanda Rojas Michaga: Writing – review & editing, Validation, Software, Methodology, Investigation. Karim Rabea: Writing – review & editing, Validation, Software, Methodology, Investigation. Kevin J Hughes: Supervision, Software, Resources. Lin Ma: Supervision, Resources. Derek Ingham: Writing – review & editing, Resources. Mohamed Pourkashanian: Supervision, Resources, Project administration.

Declaration of competing interest

The authors declare that they have no known competing financial interests or personal relationships that could have appeared to influence the work reported in this paper.

Acknowledgement

This research was funded by Center for Higher Education Funding and Assessment, Ministry of Higher Education, Science and Technology of Republik Indonesia. The second author, SM, would like to acknowledge that this work was supported by the UKRI ISCF Industrial Decarbonisation Challenge, through the UK Industrial Decarbonisation Research and Innovation Centre (IDRIC) award number: EP/V027050/1, under the Industrial Decarbonisation Challenge (IDC) and the Engineering and Physical Sciences Research Council (EPSRC) under the United Kingdom CCS Research Centre grants EP/W002841/1. We also extend our gratitude to the University of Sheffield Institutional Open Access Fund for supporting the publication costs. For the purpose of open access, the author has applied a Creative Commons Attribution (CC BY) licence to any Author Accepted Manuscript version arising.

Supplementary materials

Supplementary material associated with this article can be found, in the online version, at doi:10.1016/j.nexus.2025.100460.

Data availability

Data will be made available on request.

References

- [1] Direktorat Penanganan Sampah, Sistem Informasi Pengelolaan Sampah Nasional: SIPSN, Sistem Informasi Pengelolaan Sampah Nasional: SIPSN, 2023 [Online]. Available: https://sipsn.menlhk.go.id/sipsn/ [Accessed: 02 Jul.].
- [2] M. Vaid, et al., Microplastic pollution in aquatic environments with special emphasis on riverine systems: current understanding and way forward, J. Environ. Manag. 293 (2021) 112860, https://doi.org/10.1016/j.jenvman.2021.112860 [Online]. Available:.

- [3] W. Pang, et al., Reducing greenhouse gas emissions and enhancing carbon and nitrogen conversion in food wastes by the black soldier fly, J. Environ. Manag. 260 (2020) 110066, https://doi.org/10.1016/j.jenvman.2020.110066 [Online]. Available:.
- [4] R.K. Singh, et al., Thermal degradation of waste plastics under non-sweeping atmosphere: part 1: effect of temperature, product optimization, and degradation mechanism, J. Environ. Manag. 239 (2019) 395–406, https://doi.org/10.1016/j. jenvman.2019.03.067 [Online]. Available:.
- [5] O. Dogu, et al., The chemistry of chemical recycling of solid plastic waste via pyrolysis and gasification: state-of-the-art, challenges, and future directions, Prog. Energy Combust. Sci. 84 (2021) 100901, https://doi.org/10.1016/j. pecs.2020.100901 [Online]. Available:.
- [6] M.A. Khan, et al., Hydrothermal conversion of food waste to carbonaceous solid fuel—a review of recent developments, Foods 11 (24) (2022) 4036.
- [7] A.A. Erdogan, M.Z. Yilmazoglu, Plasma gasification of the medical waste, Int. J. Hydrog. Energy 46 (57) (2021) 29108–29125, https://doi.org/10.1016/j. ijhydene.2020.12.069 [Online]. Available:.
- [8] M. Danthurebandara, et al., Environmental and economic performance of plasma gasification in enhanced landfill mining, Waste Manag. 45 (2015) 458–467, https://doi.org/10.1016/j.wasman.2015.06.022 [Online]. Available:.
- [9] R. Mallick, V. Prabu, 4-E analyses of plasma gasification integrated chemical looping reforming system for power and hydrogen co-generation using bakelite and acrylonitrile butadiene styrene based plastic waste feedstocks, Energy Convers. Manag. 271 (2022) 116320, https://doi.org/10.1016/j.enconman.2022.116320 [Online]. Available:.
- [10] A. Mountouris, et al., Solid waste plasma gasification: equilibrium model development and exergy analysis, Energy Convers. Manag. 47 (13–14) (2006) 1723–1737, https://doi.org/10.1016/j.enconman.2005.10.015 [Online]. Available:.
- [11] P.T. Jones, et al., Enhanced landfill mining in view of multiple resource recovery: a critical review, J. Clean. Prod. 55 (2013) 45–55, https://doi.org/10.1016/j. jclepro.2012.05.021 [Online]. Available:.
- [12] D. Cudjoe, H. Wang, Plasma gasification versus incineration of plastic waste: energy, economic and environmental analysis, Fuel Process. Technol. 237 (2022) 107470, https://doi.org/10.1016/j.fuproc.2022.107470 [Online]. Available:.
- [13] L. Mazzoni, I. Janajreh, Plasma gasification of municipal solid waste with variable content of plastic solid waste for enhanced energy recovery, Int. J. Hydrog. Energy 42 (30) (2017) 19446–19457, https://doi.org/10.1016/j.ijhydene.2017.06.069 [Online]. Available:.
- [14] S. Kwon, S. Im, Thermodynamic evaluation of integrated plasma gasification combined cycle with plastic waste feedstock, Chem. Eng. J. 482 (2024) 148771, https://doi.org/10.1016/j.cej.2024.148771 [Online]. Available:.
- [15] R. Zhang, et al., Characterization of food waste as feedstock for anaerobic digestion, Bioresour. Technol. 98 (4) (2007) 929–935, https://doi.org/10.1016/j. biortech.2006.02.039 [Online]. Available:.
- [16] J. Zhang, et al., Integrating food waste sorting system with anaerobic digestion and gasification for hydrogen and methane co-production, Appl. Energy 257 (2020) 113988, https://doi.org/10.1016/j.apenergy.2019.113988 [Online]. Available:.
- [17] F. Xu, et al., Anaerobic digestion of food waste-challenges and opportunities, Bioresour. Technol. 247 (2018) 1047–1058, https://doi.org/10.1016/j. biortech.2017.09.020 [Online]. Available:.
- [18] N. Antoniou, et al., Contribution to circular Economy options of mixed agricultural wastes management: coupling anaerobic digestion with gasification for enhanced energy and material recovery, J. Clean. Prod. 209 (2019) 505–514, https://doi. org/10.1016/j.jclepro.2018.10.055 [Online]. Available:.
- [19] S.S. Laleh, et al., Thermodynamic and exergoeconomic analyses of a novel biomass-fired combined cycle with solar energy and hydrogen and freshwater production in sports arenas, Int. J. Hydrog. Energy 59 (2024) 1507–1517, https:// doi.org/10.1016/j.ijhydene.2024.02.146 [Online]. Available::
- [20] H. Athari, et al., A comparative exergoeconomic evaluation of biomass post-firing and co-firing combined power plants, Biofuels 8 (1) (2017) 1–15, https://doi.org/ 10.1080/17597269.2016.1194609 [Online]. Available:.
- [21] S. Soltani, Modified exergy and exergoeconomic analyses of a biomass post fired hydrogen production combined cycle, Renew. Energy 135 (2019) 1466–1480, https://doi.org/10.1016/j.renene.2018.09.074 [Online]. Available:.
- [22] V. Zare, Role of modeling approach on the results of thermodynamic analysis: concept presentation via thermoeconomic comparison of biomass gasificationfueled open and closed cycle gas turbines, Energy Convers. Manag. 225 (2020) 113479, https://doi.org/10.1016/j.enconman.2020.113479 [Online]. Available:.
- [23] H. Jouhara, et al., Waste heat recovery technologies and applications, Therm. Sci. Eng. Prog. 6 (2018) 268–289, https://doi.org/10.1016/j.tsep.2018.04.017 [Online]. Available:.
- [24] J. Zhang, et al., Thermodynamic analysis of SOFC–CCHP system based on municipal sludge plasma gasification with carbon capture, Appl. Energy 336 (2023) 120822, https://doi.org/10.1016/j.apenergy.2023.120822 [Online]. Available:.
- [25] J. Zhang, et al., Thermodynamic analysis of a food waste plasma gasification-based multigeneration system with dehumidification and carbon capture, J. Clean. Prod. 402 (2023) 136844, https://doi.org/10.1016/j.jclepro.2023.136844 [Online]. Available:.
- [26] B. Lemmens, et al., Assessment of plasma gasification of high caloric waste streams, Waste Manag. 27 (11) (2007) 1562–1569, https://doi.org/10.1016/j. wasman.2006.07.027 [Online]. Available:.
- [27] I. Janajreh, et al., Plasma gasification process: modeling, simulation and comparison with conventional air gasification, Energy Convers. Manag. 65 (2013) 801–809, https://doi.org/10.1016/j.enconman.2012.03.010 [Online]. Available:.

[28] N. Agon, et al., Plasma gasification of refuse derived fuel in a single-stage system using different gasifying agents, Waste Manag. 47 (2016) 246–255, https://doi. org/10.1016/j.wasman.2015.07.014 [Online]. Available:.

- [29] J.L. Shie, et al., Energy life cycle assessment of rice straw bio-energy derived from potential gasification technologies, Bioresour. Technol. 102 (12) (2011) 6735–6741, https://doi.org/10.1016/j.biortech.2011.02.116 [Online]. Available:.
- [30] P. Cui, et al., Life cycle water footprint and carbon footprint analysis of municipal sludge plasma gasification process, Energy 261 (2022) 125280, https://doi.org/ 10.1016/j.energy.2022.125280 [Online]. Available:.
- [31] K. Yin, et al., Thermodynamic and economic analysis of a hydrogen production process from medical waste by plasma gasification, Process Saf. Environ. Prot. 178 (2023) 8–17, https://doi.org/10.1016/j.psep.2023.08.007 [Online]. Available:.
- [32] H. Qi, et al., Conceptual design and comprehensive analysis for novel municipal sludge gasification-based hydrogen production via plasma gasifier, Energy Convers. Manag. 245 (2021) 114635, https://doi.org/10.1016/j. enconman.2021.114635 [Online]. Available:.
- [33] Z. Xu, et al., Exergy, techno-economic and environment analysis of food waste plasma gasification and syngas chemical looping processes, J. Clean. Prod. 386 (2023) 135835, https://doi.org/10.1016/j.jclepro.2022.135835 [Online]. Available:
- [34] P.G. Rutberg, et al., On efficiency of plasma gasification of wood residues, Biomass Bioenergy 35 (1) (2011) 495–504, https://doi.org/10.1016/j. biombioe.2010.09.010 [Online]. Available:.
- [35] S. Evangelisti, et al., Life cycle assessment of conventional and two-stage advanced energy-from-waste technologies for municipal solid waste treatment, J. Clean. Prod. 100 (2015) 212–223, https://doi.org/10.1016/j.jclepro.2015.03.062 [Online]. Available:.
- [36] S. Evangelisti, et al., Integrated gasification and plasma cleaning for waste treatment: a life cycle perspective, Waste Manag. 43 (2015) 485–496, https://doi. org/10.1016/j.wasman.2015.05.037 [Online]. Available:.
- [37] A. Ramos, et al., Life cycle costing for plasma gasification of municipal solid waste: a socio-economic approach, Energy Convers. Manag. 209 (2020) 112508, https://doi.org/10.1016/j.enconman.2020.112508 [Online]. Available:.
- [38] P. Nuss, et al., Comparative life cycle assessment (LCA) of construction and demolition (C&D) derived biomass and U.S. Northeast Forest Residuals gasification for electricity production, Environ. Sci. Technol. 47 (7) (2013) 3463–3471, https://doi.org/10.1021/es304312f [Online]. Available:.
- [39] P. Pan, et al., Design and evaluation of a conceptual waste-to-energy approach integrating plasma waste gasification with coal-fired power generation, Energy 238 (2022) 121947, https://doi.org/10.1016/j.energy.2021.121947 [Online]. Available:
- [40] Y. Ayub, et al., Plasma gasification based monetization of poultry litter: system optimization and comprehensive 5E (Energy, Exergy, Emergy, Economic, and Environmental) analysis, Energy Convers. Manag. 282 (2023) 116878, https://doi.org/10.1016/j.enconman.2023.116878 [Online]. Available:.
- [41] J. Tang, et al., From excavated waste to hydrogen: life cycle techno-environmental-economic comparison between plasma-gasification-based water gas shift and sorption enhanced water gas shift routes, Energy Convers. Manag. 292 (2023) 117375, https://doi.org/10.1016/j.enconman.2023.117375 [Online]. Available:.
- [42] W. Aich, et al., Techno-economic and life cycle analysis of two different hydrogen production processes from excavated waste under plasma gasification, Process Saf. Environ. Prot. 184 (2024) 1158–1176, https://doi.org/10.1016/j. psep.2024.02.055 [Online]. Available:.
- [43] J. Li, et al., Comparative thermodynamic and techno-economic analysis of various medical waste-to-hydrogen/methanol pathways based on plasma gasification, Appl. Therm. Eng. 221 (2023) 119762, https://doi.org/10.1016/j. applthermaleng.2022.119762 [Online]. Available:.
- [44] B. Li, et al., A novel green methanol-heat cogeneration system based on municipal solid waste plasma gasification and coke oven gas: energy, exergy, economic, and environmental assessment, Energy Convers. Manag. 311 (2024) 118510, https:// doi.org/10.1016/j.enconman.2024.118510 [Online]. Available:.
- [45] International Energy Agency, Net Zero Roadmap A Global Pathway to Keep the 1.5°C Goal in Reach, International Energy Agency, 2023 [Online]Available, http s://www.iea.org/reports/net-zero-roadmap-a-global-pathway-to-keep-the-15-oc-goal-in-reach
- [46] Core Writing Team K. Calvin, et al., IPCC, 2023: climate change 2023: synthesis report, in: H. Lee, J. Romero (Eds.), Proceedings of the Contribution of Working Groups I, II and III to the Sixth Assessment Report of the Intergovernmental Panel on Climate Change, IPCC, Geneva, Switzerland, 2023. Core Writing TeamIntergovernmental Panel on Climate Change (IPCC)[Online]Available, https://www.ipcc.ch/report/ar6/syr/ [Accessed: 5February2025].
- [47] Y. Ma, et al., Thermodynamic analysis of a carbon capture hydrogen production process for end-of-life tires using plasma gasification, J. Clean. Prod. 384 (2023) 135662, https://doi.org/10.1016/j.jclepro.2022.135662 [Online]. Available:.
- [48] D. Lu, et al., Thermo-economic analysis of a novel power system including medical-waste plasma gasification, SOFC, biomass-fired power generation, and CCS, Energy Technol. 11 (8) (2023) 2300012, https://doi.org/10.1002/ente.202300012 [Online]. Available:.
- [49] S. Chari, et al., The environmental performance of mixed plastic waste gasification with carbon capture and storage to produce hydrogen in the U.K, ACS Sustain. Chem. Eng. 11 (8) (2023) 3248–3259, https://doi.org/10.1021/ acssuschemeng.2c05978 [Online]. Available:.
- [50] P.F. Albizzati, et al., A model to assess the environmental and economic impacts of municipal waste management in Europe, Waste Manag. 174 (2024) 605–617, https://doi.org/10.1016/j.wasman.2023.12.029 [Online]. Available:.

[51] A. Rafiquee, Shabbiruddin, Optimal selection and challenges of municipal waste management system using an integrated approach: a case study, Energy Sources Part A Recov. Util. Environ. Eff. 46 (1) (2024) 1996–2023, https://doi.org/ 10.1080/15567036.2023.2298285 [Online]. Available:.

- [52] H.W. Kua, et al., Life cycle climate change mitigation through next-generation urban waste recovery systems in high-density Asian cities: a Singapore case study, Resour. Conserv. Recycl. 181 (2022) 106265, https://doi.org/10.1016/j. resconrec.2022.106265 [Online]. Available:.
- [53] PT. Sumber Organik, TPA Benowo, Surabaya. [Online]. Available: https://www.sumberorganik.com/. [Accessed: 04 Mar. 2023].
- [54] Badan Pusat Statistik Kota Surabaya, Hasil sensus penduduk 2020 kota surabaya. [Online]. Available: https://surabayakota.bps.go.id/id/pressrelease/2021/01/2 9/225/hasil-sensus-penduduk-2020-. [Accessed: 13 Mar. 2023].
- [55] S.A. Damiati, et al., Field study on adaptive thermal comfort in office buildings in Malaysia, Indonesia, Singapore, and Japan during hot and humid season, Build. Environ. 109 (2016) 208–223, https://doi.org/10.1016/j.buildenv.2016.09.024 [Online]. Available:.
- [56] V. Letschert, et al., Baseline evaluation and policy implications for air conditioners in Indonesia, in: Proceedings of the Energy Efficiency in Domestic Appliances and Lighting (EEDAL'17), 2017, pp. 81–95 [Online]. Available: 10.2760/264880.
- [57] Kementerian ESDM and Direktorat Jenderal Minyak dan Gas Bumi, 'Kapasitas penyimpanan karbon di indonesia, 30% karbon luar negeri'[Online]. Availablehttp s://migas.esdm.go.id/post/Kapasitas-Penyimpanan-Karbon-di-Indonesia-30-Karbon-Luar-Negeri[Accessed: 11October 2024].
- [58] M. Ringer, et al., Large-Scale Pyrolysis Oil Production: A Technology Assessment and Economic Analysis, National Renewable Energy Laboratory (NREL), Golden, CO., US, 2006. NREL/TP-510-37779[Online]Available, http://www.osti.gov/serv lets/purl/894989-fksp4M/ [Accessed: 24July2024].
- [59] Q. Zhang, et al., Performance analysis of municipal solid waste gasification with steam in a plasma gasification melting reactor, Appl. Energy 98 (2012) 219–229, https://doi.org/10.1016/j.apenergy.2012.03.028 [Online]. Available:.
- [60] M. Minutillo, et al., Modelling and performance analysis of an integrated plasma gasification combined cycle (IPGCC) power plant, Energy Convers. Manag. 50 (11) (2009) 2837–2842, https://doi.org/10.1016/j.enconman.2009.07.002 [Online]. Available:.
- [61] C.J. Banks, et al., Anaerobic digestion of source-segregated domestic food waste: performance assessment by mass and energy balance, Bioresour. Technol. 102 (2) (2011) 612–620, https://doi.org/10.1016/j.biortech.2010.08.005 [Online]. Available:.
- [62] S. Michailos, et al., Biomethane production using an integrated anaerobic digestion, gasification and CO2 biomethanation process in a real waste water treatment plant: a techno-economic assessment, Energy Convers. Manag. 209 (2020) 112663, https://doi.org/10.1016/j.enconman.2020.112663 [Online]. Available:.
- [63] P. Cozma, et al., Modeling and simulation of high pressure water scrubbing technology applied for biogas upgrading, Clean Technol. Environ. Policy 17 (2) (2015) 373–391, https://doi.org/10.1007/s10098-014-0787-7 [Online]. Available:
- [64] T. Kreutz, et al., Fischer-Tropsch fuels from coal and biomass, in: Proceedings of the 25th Annual International Pittsburgh Coal Conference, Pittsburgh, Pennsylvania, USA, 2008.
- [65] L.R. Clausen, et al., Technoeconomic analysis of a low CO2 emission dimethyl ether (DME) plant based on gasification of torrefied biomass, Energy 35 (12) (2010) 4831–4842, https://doi.org/10.1016/j.energy.2010.09.004 [Online]. Available:.
- [66] N. Kuehn et al., 'Current and future technologies for natural gas combined cycle (NGCC) power plants', NETL/DOE-341/061013, 1490262, 2013[Online]. Availablehttps://www.osti.gov/servlets/purl/1490262/[Accessed: 24July2024].
- [67] C. Somers, et al., Modeling water/lithium bromide absorption chillers in ASPEN Plus, Appl. Energy 88 (11) (2011) 4197–4205, https://doi.org/10.1016/j.apenergy.2011.05.018 [Online]. Available:.
- [68] G.T. Udeh, et al., A techno-enviro-economic assessment of a biomass fuelled micro-CCHP driven by a hybrid Stirling and ORC engine, Energy Convers. Manag. 227 (2021) 113601, https://doi.org/10.1016/j.enconman.2020.113601 [Online]. Available:.
- [69] M. Kanoglu, et al., Performance analysis of gas liquefaction cycles, Int. J. Energy Res. 32 (1) (2008) 35–43, https://doi.org/10.1002/er.1333 [Online]. Available:.
 [70] Electric Power Research Institute and W. Elliott, 'Front-end engineering design
- (FEED) study for a carbon capture plant retrofit to a natural gas-fired gas turbine combined cycle power plant (2x2x1 Duct-Fired 758-MWe facility with F class turbines)', DOE-BECHTEL-FE0031848-App.Volume, 1836563, 2021[Online]. Availablehttps://www.osti.gov/servlets/purl/1836563/[Accessed: 24July2024].
- [71] A. Kumar, S.R. Samadder, Development of lower heating value prediction models and estimation of energy recovery potential of municipal solid waste and RDF incineration, Energy 274 (2023) 127273, https://doi.org/10.1016/j. energy.2023.127273 [Online]. Available:.
- [72] J. Szargut, Exergy Method: Technical and Ecological Applications, WIT Press, Southampton; Boston, 2005.
- [73] J. Szargut et al., 'Exergy analysis of thermal, chemical, and metallurgical processes', 1987.
- [74] Biomass Gasification and Pyrolysis, Elsevier, 2010 [Online]Available, https:// linkinghub.elsevier.com/retrieve/pii/C20090200997 [Accessed: 20November 2024].
- [75] J. Liu, et al., Improving urban ecosystem holistic sustainability of municipal solid waste-to-energy strategy using extended exergy accounting analysis, Sci. Total Environ. 904 (2023) 166730, https://doi.org/10.1016/j.scitotenv.2023.166730 [Online]. Available:.

[76] J. Liu, et al., Extended exergy accounting theory to design waste-to-energy management system under uncertainty, Energy 278 (2023) 127924, https://doi. org/10.1016/j.energy.2023.127924 [Online]. Available:.

- [77] A.H. Hendo, S. Sanaye, Simultaneous economic and exergetic optimization of a municipal solid waste incineration plant for sustainable power generation, Energy 293 (2024) 130713, https://doi.org/10.1016/j.energy.2024.130713 [Online]. Available:.
- [78] G. Diaz, et al., Enhanced hydrogen production using steam plasma processing of biomass: experimental apparatus and procedure, Int. J. Hydrog. Energy 40 (5) (2015) 2091–2098, https://doi.org/10.1016/j.ijhydene.2014.12.049 [Online]. Available:.
- [79] Q. Zhang, et al., A thermodynamic analysis of solid waste gasification in the plasma gasification melting process, Appl. Energy 112 (2013) 405–413, https://doi.org/ 10.1016/j.apenergy.2013.03.054 [Online]. Available:.
- [80] C. Banks et al., 'Food waste digestion: anaerobic digestion of food waste for a circular economy', 2018.
- [81] E. Bellos, et al., Exergetic, energetic and financial evaluation of a solar driven absorption cooling system with various collector types, Appl. Therm. Eng. 102 (2016) 749–759, https://doi.org/10.1016/j.applthermaleng.2016.04.032 [Online]. Available:.
- [82] M. T. Nitsas and I. P. Koronaki, 'A study on the performance of solar driven absorption chiller in terms of coefficient of performance and exergy efficiency', in Volume 8A: Energy, Virtual, Online, 2021, p. V08AT08A004[Online]. Availablehtt ps://asmedigitalcollection.asme.org/IMECE/proceedings/IMECE2021/85635/V0 8AT08A004/1132921[Accessed: 22July2024].
- [83] A.A.V. Ochoa, et al., Energetic and exergetic study of a 10RT absorption chiller integrated into a microgeneration system, Energy Convers. Manag. 88 (2014) 545–553, https://doi.org/10.1016/j.enconman.2014.08.064 [Online]. Available:.
- [84] S. Michailos, J. Gibbins, A modelling study of post-combustion capture plant process conditions to facilitate 95-99% CO2 capture levels from gas turbine flue

- gases, Front. Energy Res. 10 (2022) 866838, https://doi.org/10.3389/fenrg.2022.866838 [Online]. Available:.
- [85] S. Michailos, et al., A performance modeling study for zero fossil CO2 Stack operation and solvent thermal reclaiming in post-combustion capture industrial applications, Ind. Eng. Chem. Res. 64 (13) (2025) 7100–7114, https://doi.org/ 10.1021/acs.iecr.4c04530 [Online]. Available:.
- [86] P. Jiang, et al., Novel two-stage fluidized bed-plasma gasification integrated with SOFC and chemical looping combustion for the high efficiency power generation from MSW: a thermodynamic investigation, Energy Convers. Manag. 236 (2021) 114066, https://doi.org/10.1016/j.enconman.2021.114066 [Online]. Available:.
- [87] N.D. Montiel-Bohórquez, et al., Effect of origin and production rate of MSW on the exergoeconomic performance of an integrated plasma gasification combined cycle power plant, Energy Convers. Manag. 238 (2021) 114138, https://doi.org/ 10.1016/j.enconman.2021.114138 [Online]. Available:.
- [88] M. Elwardany, et al., Energy and exergy assessment of 750 MW combined cycle power plant: a case study, Energy Nexus 12 (2023) 100251, https://doi.org/ 10.1016/j.nexus.2023.100251 [Online]. Available:.
- [89] A. Almutairi, et al., Energetic and exergetic analysis of combined cycle power plant: part-1 operation and performance, Energies 8 (12) (2015) 14118–14135, https://doi.org/10.3390/en81212418 [Online]. Available:.
- [90] G. Ferrara, et al., Exergetic and exergoeconomic analysis of post-combustion CO2 capture using MEA-solvent chemical absorption, Energy 130 (2017) 113–128, https://doi.org/10.1016/j.energy.2017.04.096 [Online]. Available:.
- [91] W.S. Lee, et al., Performance, economic and exergy analyses of carbon capture processes for a 300 MW class integrated gasification combined cycle power plant, Energy 134 (2017) 731–742, https://doi.org/10.1016/j.energy.2017.06.059 [Online]. Available:.
- [92] N. Xie, et al., Energy consumption and exergy analysis of MEA-based and hydrate-based CO₂ separation, Ind. Eng. Chem. Res. 56 (51) (2017) 15094–15101, https://doi.org/10.1021/acs.iecr.7b03729 [Online]. Available:.